Pergamon

Bioorganic & Medicinal Chemistry 8 (2000) 1225–1243

BIOORGANIC & MEDICINAL CHEMISTRY

Lincomycin and Clindamycin Conformations. A Fragment Shared by Macrolides, Ketolides and Lincosamides Determined from TRNOE Ribosome-Bound Conformations

Laurent Verdier,[a] Gildas Bertho,[a] Josyane Gharbi-Benarous[a,b] and Jean-Pierre Girault[a,*]

[a]*Université René Descartes-Paris V, Laboratoire de Chimie et Biochimie Pharmacologiques et Toxicologiques (UMR 8601 CNRS), 45 rue des Saint-Pères, 75270 Paris Cedex 06, France*

[b]*Université Denis Diderot-Paris VII, UFR Chimie, 2 Place Jussieu, 75251 Paris cedex 05, France*

Received 27 September 1999; accepted 22 December 1999

Abstract—Two important lincosamide antibiotics, lincomycin and clindamycin were studied in the complex state with the bacterial ribosome after a conformational analysis by ^{1}H and ^{13}C NMR spectroscopy and molecular modelling of the unbound molecules. Lincosamide-ribosome interactions were investigated using two-dimensional transferred nuclear Overhauser effect spectroscopy (TRNOESY), resulting in a bound structure compatible with the experimental NMR data. The results compared with the conformational analysis of the substrates in solution indicate that specific conformations are preferred in the bound state. Clindamycin, the more bioactive antibiotic studied, displayed a stronger NMR response than lincomycin showing that in lincosamide-ribosome interactions, a low affinity binding level is associated to the tight binding one and is related to biological activity. This study shows that conformation plays an essential role for the low affinity binding site. Superimposition of lincosamide, macrolide and ketolide bound structures exhibited conformational similarities in a particular fragment which is in agreement with a hypothesis of partial overlapping lincosamide and macrolide binding sites.

Introduction

Lincomycin (**1**) and clindamycin (**2**) are lincosamide antibiotics widely used in clinical practice against gram-positive microorganisms. Lincomycin is produced naturally by several species of actinomycetes, *Streptomyces lincolnensis*, *espinosus*, and *Actinomyces roseolus*, and clindamycin is a semisynthetic derivative obtained by chlorination of lincomycin.[1,2] Small modifications at carbon-7 or loss of the carbonyl group caused dramatic alterations in lincomycin activity.[3] Clindamycin is approximately 20 times more effective than lincomycin in inhibiting the growth of *Escherichia coli*.[4]

(1) Lincomycin R_1= OH R_2= H

(2) Clindamycin R_1= H R_2= Cl

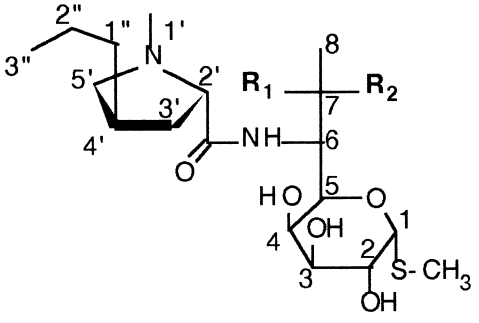

The search for antibiotics active against MLS_B (macrolide-lincosamide-streptogramin B) resistant strains has become a major goal, together with retaining the overall profile of the MLS antibiotics in terms of stability, tolerance and pharmacokinetics. Several antibiotics including 14-membered macrolides like erythromycin and roxithromycin, 16-membered macrolides like spiramycin and josamycin, and lincosamides like lincomycin (**1**) and clindamycin (**2**) inhibit protein synthesis by interfering with the peptidyl-transferase function of the 50S ribosomal subunit.[5–7] Ribosomal L proteins and

*Corresponding author. Tel.: +33-1-42-86-21-80; fax: +33-1-42-86-83-87; e-mail: girault j@biomedicale.univ-paris5.fr

0968-0896/00/$ - see front matter
PII: S0968-0896(00)00081-X

portions of 23S rRNA have both been identified at the catalytic centre of the peptidyl-transferase.[8–10] The study of certain cases of microbial resistance to antibiotics has shed light on the topology of the peptidyl-transferase domain on the 50S ribosomal subunit, the common target of the MLS_B group of antibiotics.[5] The spatial distribution of the different binding sites for (i) streptogramin B and macrolides, and (ii) lincosamides involves their partial overlapping.[4,7]

In this article, we try to shed light on the conformation of lincomycin (**1**) and clindamycin (**2**) bound to bacterial ribosomes, beyond what is already known on the mechanism of action of lincosamides and macrolides.

(i) Macrolide antibiotics like erythromycin A and roxithromycin inhibit protein biosynthesis in the elongation step by binding to the 50S bacterial ribosome. There appear to be two stages to this binding: a weak interaction which can be detected by NMR spectroscopy,[11,12] and a stronger one.[13–15] Taking advantage of the exchange between bound and free macrolide antibiotics, we have previously studied the weak interactions of *E. coli* ribosomes with macrolides of the 14-membered ring class {erythromycin, roxithromycin, clarithromycin,..}, the 16-membered ring class {josamycin,..}[16] and the new class of antibiotics called ketolides {HMR 3004 (RU 004), telithromycin (HMR 3647),..},[17,18] using line broadening and transferred NOESY (TRNOESY) experiments.[11,19–21] TRNOE NMR experiments proved to be efficient for the location and detection of weak interactions due to ribosomal activity, providing a means to study the relationship between the conformations of antibiotics when interacting and their activity. In this study, TRNOESY experiments were extended to lincomycin (**1**) and clindamycin (**2**).

(ii) It was noticed that lincosamides generally showed a slightly lower affinity for the 70S ribosome target than did erythromycin,[22] but displayed significantly good overall antibiotic activity. The dissociation constants for lincomycin (**1**) and clindamycin (**2**) tight binding were estimated to be 5×10^{-6} and 8×10^{-6} M, respectively.[4] Earlier work[23,24] on the strong interactions of lincomycin has given rise to the conclusion that lincomycin and streptogramin A only interact with free ribosomes and 50S subunits and block the early rounds of peptide bond formation prior to polysome formation, while erythromycin and streptogramin B prebind to the ribosome and block peptide elongation.

In order to compare the behaviour of lincosamides, their conformations when weakly bound to bacterial ribosomes were determined. Moreover, in the ribosome complex, from the constraints of the different TRNOEs observed in D_2O, we proposed to analyse whether the lincosamide and 14-membered macrolide families present a shared bound region or if the conformations when weakly bound to bacterial ribosomes vary.

The primary goal of this work was to determine the overall solution conformation of lincomycin (**1**) and clindamycin (**2**).

Results and Discussion

A NMR and MD study of lincomycin (**1**) and clindamycin (**2**) will be developed here, in order to explore fully the conformational space of these compounds and to understand the structure–activity relationship of lincosamides. Their different inhibitory activities observed against *E. coli*, would be due to structural differences, localized flexibility, minor conformers or a particular transition state implied in the reaction with the ribosome.

The site of lincomycin action was located on the 50S ribosomal subunits and hydrophobic interactions could play an essential role in the binding of lincomycin to ribosomes since it was found that *N*-demethyllincomycin was only 10% as active as the parent compound.[23] Considering the interaction between lincosamides and ribosome, the different functional groups, namely the amide group, the 7-OH, the 4-OH, O(1) in addition to the C(4′)-substituent (propyl group) should be adequately arranged to favourably fit into the receptor. The pyrrolidine ring should play a role to arrange the spatial position of these functional groups in the molecules.

Whether the major conformation populated in solution is likely to be the ribosome bound one or whether high energy conformation populated in solution will be the ribosome bound one.

Conformational analysis of the free ligands

The conformational analysis of the **1**–**2** compounds in solution was difficult to elucidate because of their structural characteristics resulting in additional flexible moieties (Figs 1 and 2). In the present article, we propose an accurate description of rings, pyrrolidine and pyranose and the correlated conformations of the C(6)–C(8) side chain (Table 1).

(i) The preferred conformer of the pyranose is the *chair* form in which the energy barrier to convert a *chair* form $^4\mathbf{C_1}$ into another one $_4\mathbf{C^1}$ (Fig. 1a) is relatively high. The *chair* form $^4\mathbf{C_1}$ of the pyranose is considered 'rigid'.

(ii) The conformation of the 5-membered ring, pyrrolidine unprotonated and protonated (at pyrrolidine nitrogen, N(1′)) forms, is best described using the pseudorotational circle (Fig. 1b). Two flexible forms exist, namely *envelope* **E** and *half-chair* or twist **T** conformers. The envelope and the half chair forms interconvert by the pseudorotation process but in the pyrrolidine ring the presence of the three substituents, will give rise to an induced potential energy barrier opposing free pseudorotation.

(iii) The moiety (C(5)–C(6)–C(7)–C(8)) presents a partially restricted rotation around the C(5)–C(6) (χ_1) and C(6)–C(7) (χ_2) bonds (Fig. 2a). The C(5)–C(6)–C(7) system allows the possibility of *trans* and *gauche* forms and nine staggered conformations **G1**–**G9** (Fig. 2b) result from the combination of the "t, g^+, g^-" rotamers about χ_1 and χ_2. It was of interest to identify which of those **G1**–**G9** conformations (tt, tg^+, tg^-, ...) corresponds to the **1** and **2** structure and is able to fit to the receptor.

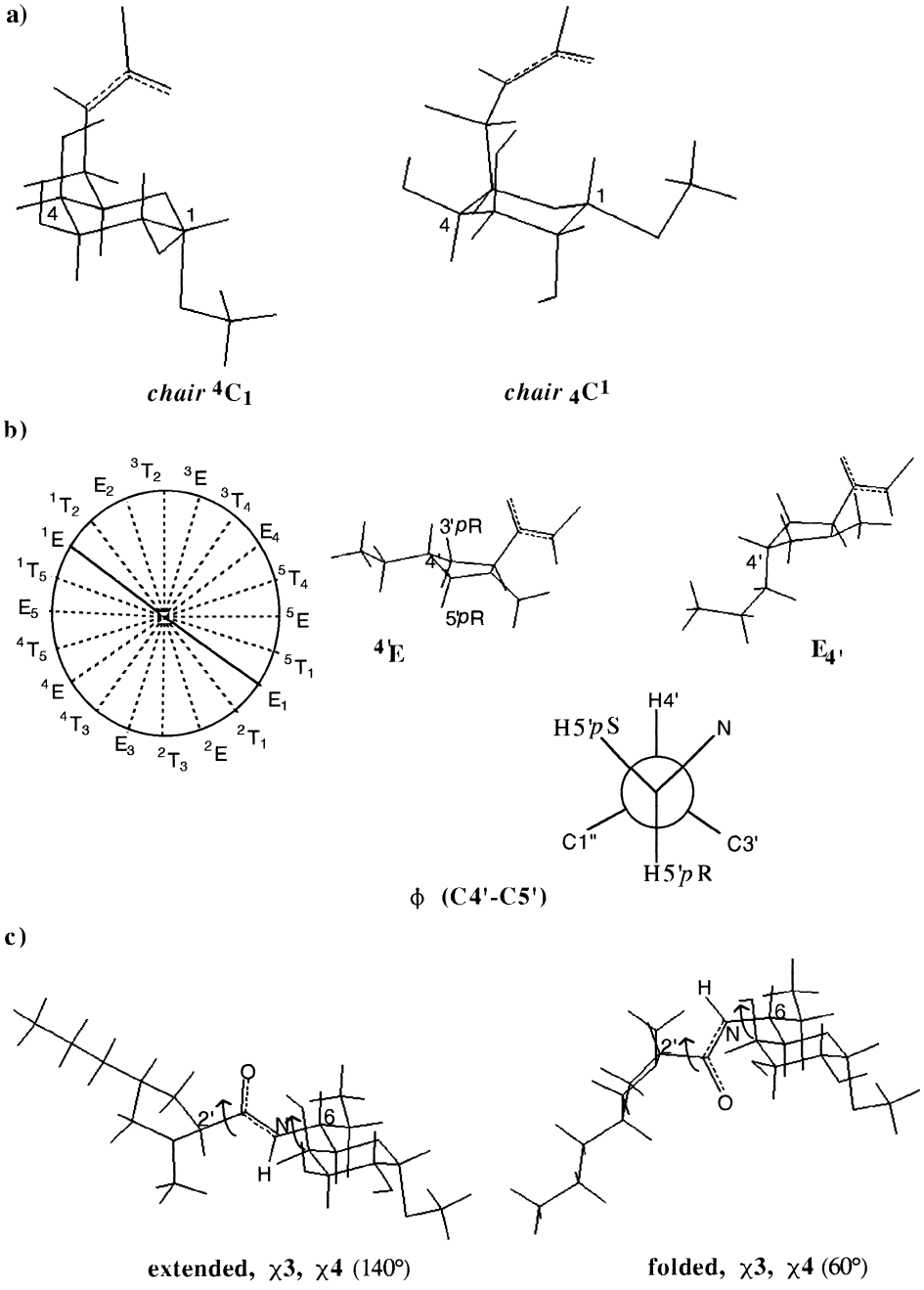

Figure 1. (a) $^4C_1$ and $_4C^1$ chair conformations for the galacto-octopyranoside ring. (b) Pseudorotational pathway of cyclopentane ring for propyl-pyrrolidinyl ring. Each external point of dotted radials in the circle represents a specific *envelope* **E** and *half-chair* or *twist* **T** conformation. Conformational equilibrium between the structure $^{4'}$**E** and another envelope $\mathbf{E}_{4'}$ when the out-of-plane carbon C-4′ is pushed down. Newman projection relative to the torsion angle ϕ [C(4′)–C(5′)] (viewed in the C(5′)→C(4′) direction). (c) The amide bond between the cyclohexane or cyclopentane fragment was fixed in the *trans* geometry, but the side chain around (χ_3) (C(6)–NH–CO) and (χ_4) (C(2′)–CO–NH) was flexible: the extended structures corresponding to (χ_3) and (χ_4) dihedral angle values of ±140° or ±120° were more stable than those having (χ_3) and (χ_4) ±60°.

(iv) For the amide unit, the free rotation around the (C(5)–C(6)–NH–CO) (χ_3) bond corresponds to the conformational relationship between the carbohydrate moiety and the amide unit and the dihedral (C(3′)–C(2′)–CO–NH) (χ_4) specifies the conformational relationship between the pyrrolidine ring and the amide unit, *eclipsed* or *anti* (Fig. 1c).

(v) The hydrocarbon side chain (C(4′)–C(1″)–C(2″)–C(3″)) attached to the pyrrolidine ring at the 4′ position leads to the fluctuate angles (χ_5) (C(4′)–C(1″) and (χ_6) (C(1″)–C(2″)) with a high degree of liberty (Fig. 2c). This allows the possibility of the staggered conformations **C1**–**C9** (*tt*, tg^+, tg^-, ...) (Fig. 2d). These nine conformations are observed according to the ten *envelopes* (**P1**–**P10**) of the 5-membered ring.

In order to gain some insight into lincomycin (**1**) and clindamycin (**2**) possible conformations, we have undertaken their conformational analysis by 1D ^{1}H and

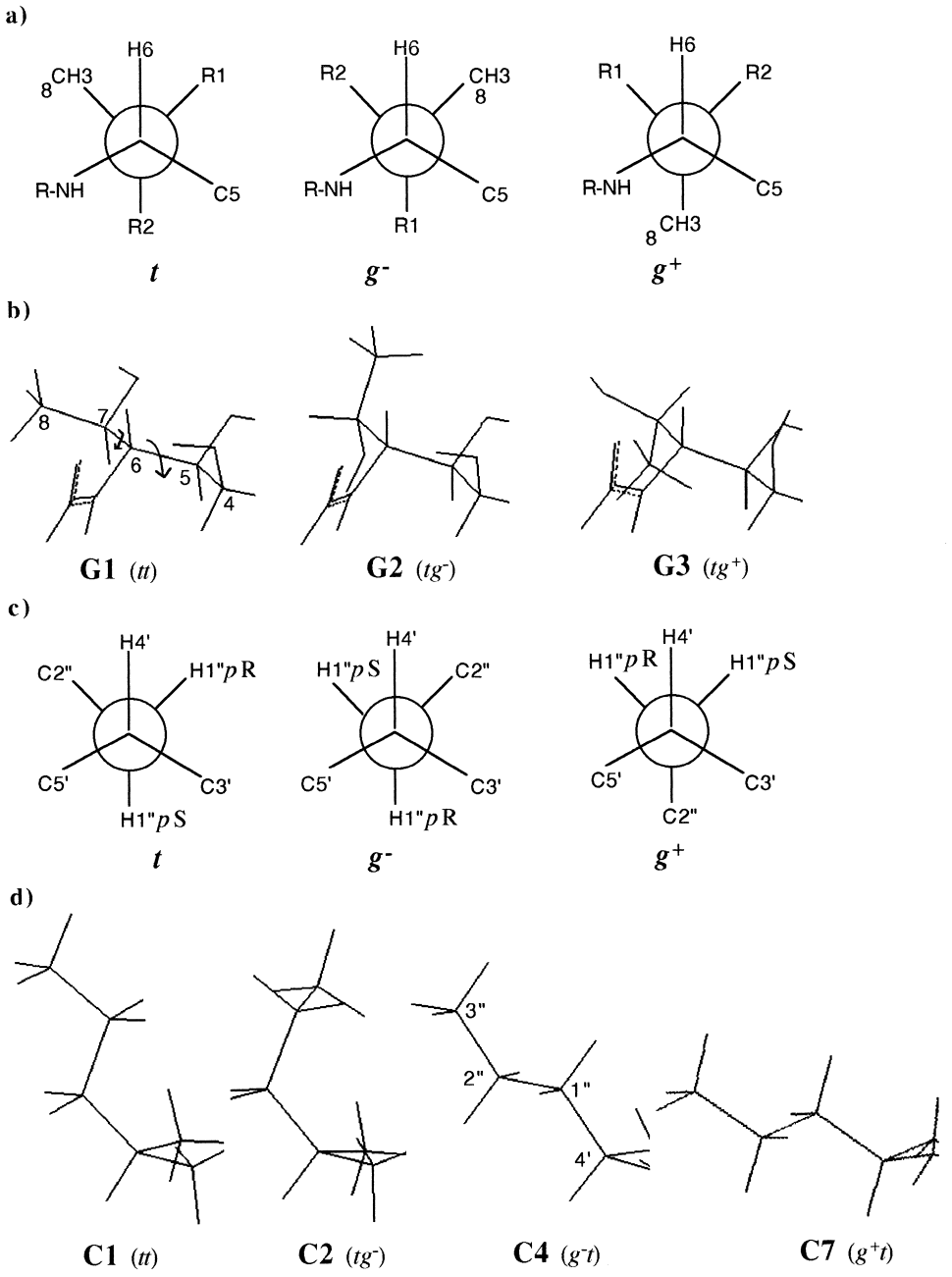

Figure 2. (a) Newman projections for the three "staggered" rotamers '*t*, g^-, g^+' relative to the torsion angle χ_2 (C(6)–C(7)) (viewed in the C(6)→C(7) direction). (b) Three structures **G1**–**G3** are represented here from the nine conformations **G1**–**G9** resulting of the combination of the rotamers '*t*, g^-, g^+' relative to the torsion angles χ_1 (C(5)–C(6)) and χ_2 (C(6)–C(7)). (c) Newman projections for the three rotamers '*t*, g^-, g^+' relative to the torsion angle χ_5 (C(4′)-C(1″)) (viewed in the C(4′)→C(1″) direction). (d) Four structures **C1** (*tt*), **C2** (tg^-), **C4** (g^-t) and **C7** (g^+t) are represented here from the nine conformations **C1**–**C9** resulting from the combination of the rotamers '*t*, g^-, g^+' relative to the torsion angle χ_5 (C(4′)–C(1″)) and χ_6 (C(1″)–C(2″)).

^{13}C NMR, 2D NMR techniques (^{1}H-^{1}H COSY, NOESY and 2D gradient-selected *J*-HMBC) and molecular modelling. As molecular dynamic (MD) calculations deal with the energy and geometry of individual conformations, whereas NMR data are averaged over different conformations, this study serves to correlate the two methods.

We have extended the MD study to the charged pyrrolidinium cation, so as not to neglect the protonation site which will induce particular conformations. The final structures obtained after several MD calculations were examined for the overall energetic favorability and compared with the structure derived from the NMR data. The torsion angles of generated structures can be correlated with the corresponding coupling constants by using Karplus type-equations.[25,26] The agreement of the generated structures with the experimental NMR coupling constants is then examined.

Table 1. Notation for conformer designations defined as '**G1–G9**, **P1–P10** and **C1–C9**'

Galacto-octopyranoside sugar fragment (C(4)–C(5)–C(6)–C(7)–C(8))										
			χ_1 ((C(5),C(6))							
χ_2 ((C(6),C(7))			*t* (180°)			g^- (−60°)			g^+ (+60°)	
t (180°)			[**G1** (*tt*)]			[**G4** (g^-t)]			[**G7** (g^+t)]	
g^- (−60°)			**G2** (tg^-)			**G5** (g^-g^-)			**G8** (g^+g^-)	
g^+ (+60°)			**G3** (tg^+)			**G6** (g^-g^+)			**G9** (g^+g^+)	
*Proline fragment (1-methyl-*n*-propylproline)*										
	P1	**P2**	**P3**	**P4**	**P5**	**P6**	**P7**	**P8**	**P9**	**P10**
Envelopes	$^{3'}$E	$E_{4'}$	$^{5'}$E	$E_{1'}$	$^{2'}$E	$E_{3'}$	$^{4'}$E	$E_{5'}$	$^{1'}$E	$E_{2'}$
Chain fragment (n-*propyl side chain (C(4′)–C(1″)–C(2″)–C(3″))*										
			χ_5 ((C(4′),C(1″))							
χ_6 ((C(1″),C(2″))			*t* (180°)			g^- (−60°)			g^+ (+60°)	
t (180°)			[**C1** (*tt*)]			[**C4** (g^-t)]			[**C7** (g^+t)]	
g^- (−60°)			**C2** (tg^-)			**C5** (g^-g^-)			**C8** (g^+g^-)	
g^+ (+60°)			**C3** (tg^+)			**C6** (g^-g^+)			**C9** (g^+g^+)	

Table 2. ^{1}H and ^{13}C NMR chemical shifts (δ in ppm) for lincomycin (**1**) and clindamycin (**2**) in D_2O buffered solution (4 mM) at pH 7.6

	Lincomycin (**1**)		Clindamycin (**2**)	
Site	δ_H	δ_C	δ_H	δ_C
1	5.38	91.0	5.42	90.6
1-SMe	2.15	15.8	2.20	15.5
2	4.13	70.5	4.14	70.5
2-OH[a]	5.12		5.18	
3	3.66	73.1	3.69	73.2
3-OH[a]	4.89		4.98	
4	3.93	71.2	3.90	70.9
4-OH[a]	4.74		4.77	
5	4.23	71.8	4.37	71.8
6	4.41	53.2	4.47	55.8
6-CO		172.4		172.4
6-NH[a]	8.22		8.64	
7	4.18	69.3	4.63	60.7
7-OH[a]	4.63		—	
8-Me	1.17	18.5	1.44	24.5
1′-Me	2.86	43.3	2.85	43.4
1′-NH[a]	9.68		9.74	
2′	4.11	71.2	4.12	71.1
3′-a (*pro*S)	2.23	38.4	2.28	38.7
3′-b (*pro*R)	2.28		2.28[b]	
4′	2.40	39.3	2.37	39.3
5′-a (*pro*S)	3.75	64.2	3.75	64.3
5′-b (*pro*R)	2.80		2.78	
6′	1.46	37.0	1.46	37.0
7′	1.33	23.3	1.33	23.3
8′	0.90	16.0	0.90	16.0

[a]Solution in DMSO (4 mM).
[b]Isochronous.

NMR spectroscopy

The ^{1}H and ^{13}C NMR chemical shifts in aqueous NaD_2PO_4/Na_2DPO_4 buffer (0.05 M), with KCl (0.2 M) at physiological apparent pH 7.6 for (**1**–**2**) are listed in Table 2. The $^3J_{HH}$ values used to evaluate solution conformation are given in Table 3. To determine the overall pyrrolidine conformation it was necessary to obtain more information about the spatial proximity of proton pairs in solution from the observed NOEs found in 2D phase sensitive ^{1}H NOESY (Table 4).

Assignments. The assignments were made using 1D ^{1}H and ^{13}C (^{1}H decoupled and DEPT-135) spectra[27] and ^{1}H-^{13}C Chemical Shift Correlation (PFG-HMQC and HMBC, Pulse Field Gradient-Heteronuclear Multiple-Quantum Correlation[28] and multiple bond correlation[29]) spectra.

From ^{1}H NMR spectrum at 500.13 MHz and ^{1}H-^{1}H Chemical Shift Correlation (COSY), the chemical shift (5.38 ppm) of the 1-H (because of the adjacent O and S atoms) provides the starting point for tracing the coupling partners. A spin-coupling network is observed for the protons: 1-H, 2-H, 3-H, 4-H, 5-H, 6-H, 7-H, 8-H and NH, which provides unambiguous assignments of these protons. The complete assignment of the ^{1}H and ^{13}C signals was achieved except for the attribution of the diastereotopic protons (3′a, 3′b and 5′a, 5′b). The prefixes *R* and *S* are used to unambiguously designate the configuration of prochiral centers.

From the assigned ^{13}C spectrum, the ^{1}H-^{13}C spectra provided a facile and straightforward identification of the chemical shifts of each proton by correlating the carbon–proton resonances: the chemical shifts of the two diastereotopic 3′a-H and 3′b-H protons are respectively 2.23 and 2.28 ppm and those of 5′a-H, 5′b-H protons are respectively 3.75 and 2.80 ppm.

The assignment of the individual diastereotopic methylene protons was particularly difficult.[30,31] The homonuclear coupling constants and the NOE experiments are not sufficient to allow unambiguous assignments. It was necessary to define the $^3J_{(C,H)}$ coupling constants of both diastereotopic protons at C(3′) and C(5′) by the 2D gradient-selected *J*-HMBC[32] and use these values in conjunction with $^3J_{(H,H)}$ to define the conformation of the C(2′)–C(3′)–C(4′)–C(5′) fragment (Table 3). In the Newman projection (Fig. 1b), as $5'_R$-H is *trans* to 4′-H, and *gauche* to the carbon 3′-C and 2′-C, the experimental NMR data from 5′b-H ($^3J_{4',5'b}$ large when $^3J_{4',5'a}$, $^3J_{C(2')H(5'b)}$ and $^3J_{C(3')H(5'b)}$ are small) allow us to assign 5′b-H to 5′-H_R. The position of the 3′-H relative to the face of the 5-membered ring is defined by the observed NOEs involving 3′a-H (3′a-H and 1′-Me are located in the same face) (Figs 1b and 3). We can also

Table 3. Experimental constants obtained by NMR and calculated coupling constants (in parentheses) corresponding to some torsion angles of structures computed by MD for lincomycin (**1**) and clindamycin (**2**)

	J/Hz		Torsion angle (°C) (and ^3J/Hz)						
Pyranoside	(**1**)	(**2**)	*chair* $^4\mathbf{C_1}$	*chair* $_4\mathbf{C^1}$					
H1–H2	5.8	5.8	51 (4.5)	−53 (4.3)					
H2–H3	10.3	10.4	−174 (13.2)	−70 (2.3)					
H3–H4	3.1	3.2	52 (4.4)	−50 (4.7)					
H4–H5	0.7	1.1	−55 (4)	35 (6.9)					
H1–C3	6.2	6.1	171 (6.6)	69 (1.0)					
H1–C5	6.8	6.7	178 (6.8)	−67 (1.1)					
H1–SCH_3	3.5	2.9	[a]	[a]					
χ1 (C(5),C(6))	(**1**)	(**2**)							
H5–H6	9.7	10.1	−176 (12.4)	−57 (3.7)	68 (2.4)				
H5–C7	≈1	1.8	−61 (1.5)	59 (1.7)	−173 (6.7)				
H6–C4	≈1	∼2	64 (1.3)	−177 (6.8)	−47 (2.7)				
χ2 (C(6),C(7))	(**1**)	(**2**)							
H6–H7	4.3	1.2	177 (12.4)	−60 (3.3)	66 (2.6)				
H7–C5	≈1	≈1	57 (1.9)	−174 (6.7)	−49 (2.5)				
H6–C8	4.2	≈0.7	52 (2.3)	176 (6.8)	−54 (2.1)				
H7–N	Large	Large	−63 (2.5)	50 (3.5)	−177 (10.0)				
Peptide bond χ3 (C(6),NH)	(**1**)	(**2**)							
H6–NH	9.0	7.0	[b]						
H6–CO	3.2	3.1	[b]						
Proline	(**1**)	(**2**)	**P1** ($^{3'}$E)	**P2** ($E_{4'}$)	**P3** ($^{5'}$E)	**P4**($E_{1'}$)	**P5** ($^{2'}$E)	**P6** ($E_{3'}$)	**P7** ($^{4'}$E)
H2′–H3′a(*p*S)	9.3	8.8	31 (7.5)	16 (9.1)	5 (9.7)	−37 (6.6)	−44 (5.6)	−44 (5.6)	−33 (7.2)
H2′–H3′b(*p*R)	6.4	6.7	−88 (1.6)	−102 (2.3)	−113 (3.6)	−155 (10.6)	−163 (11.5)	−164 (11.6)	−152 (10.1)
H3′a(*p*S)–H4′	9.2	9.2	−164 (11.6)	−164 (11.6)	−161 (11.3)	−122 (4.9)	−99 (2.0)	−86 (1.5)	−86 (1.5)
H3′b(*p*R)–H4′	8.4	8.4	−45 (5.4)	−45 (5.4)	−42 (5.9)	−4 (9.7)	19 (8.9)	32 (7.3)	31 (7.5)
H4′–H5′a(*p*S)	6.8	6.8	27 (8.0)	46 (5.3)	47 (5.1)	31 (7.5)	2 (9.8)	−19 (8.9)	−31 (7.5)
H4′–H5′b(*p*R)	10	9.7	147 (9.4)	167 (11.9)	168 (12.0)	150 (9.8)	120 (4.6)	99 (2.0)	88 (1.6)
H4′–C2′	≈1	0.9	79 (0.6)	79 (0.6)	82 (0.5)	116 (1.9)	138 (4.1)	151 (5.4)	150 (5.3)
H2′–C4′	≈1	3.3	149 (5.2)	134 (3.7)	124 (2.6)	87 (0.5)	80 (0.6)	79 (0.6)	91 (0.5)
H2′–C(me)1′	3.8	3.4	77 (0.7)	28 (4.4)	32 (4.1)	157 (5.9)	52 (2.3)	43 (3.1)	103 (0.9)
H2′–C5′	≈1	≈1	−137 (3.9)	−107 (1.2)	−97 (0.6)	−73 (0.8)	−80 (0.6)	−91 (0.5)	−114 (1.7)
H5′a(*p*S)–C2′	6.8	6.7	−118 (2)	−152 (5.5)	−156 (5.8)	−159 (6.0)	−139 (4.2)	−118 (2.0)	−93 (0.5)
H5′a(*p*S)–C3′	6.7	6.7	141 (4.4)	159 (6.0)	159 (6.0)	144 (4.7)	116 (1.9)	96 (0.6)	82 (0.5)
H5′b(*p*R)–C2′	[c]	[c]	124 (2.6)	89 (0.5)	85 (0.5)	83 (0.5)	104 (1.0)	125 (2.7)	149 (5.2)
H5′b(*p*R)–C3′	≈1	[c]	−99 (0.7)	−80 (0.6)	−80 (0.6)	−98 (0.7)	−126 (2.8)	−147 (5.0)	−158 (6.0)

[a] $\phi_{H1,SCH3}$ (−48°)–(−56°), *J* (≈2.5 Hz).
[b] $\phi_{H6,NH}$ (140°)–(180°), *J* (≈9.5 Hz); $\phi_{H6,CO}$ (−30°)–(+30°), *J* (≈4.5 Hz).
[c] Overlapping.

deduce the axial or equatorial position of 3′a-H and 5′b-H from the spin system value of the neighbouring nucleus 4′-H. The value of $^3J_{4',5'b}$ (10 Hz) and $^3J_{4',3'a}$ (9.2 Hz) show that 5′b-H, 3′a-H and 4′-H are axial and thus 5′b-H and 5′a-H were assigned to *R* and *S*, respectively and 3′b-H and 3′a-H to *R* and *S*, respectively.

Conformation of the pyrrolidine and pyranose rings. The conformational analysis is based on the vicinal $^3J_{1_H,1_H}$ and $^3J_{13_C,1_H}$ coupling constants reported in Table 3. The pyranose ring in **1** and **2** always adopts the chair conformation $^4\mathbf{C_1}$ with 5-chain moiety equatorial and the minimal sterical hindrance (Fig. 1a). Using the extreme value of the coupling constant $^3J_{2ax,3ax} = 10$ Hz, it is possible to estimate that the $^4\mathbf{C_1}$ conformer is predominant being very likely stabilized by hydrogen bonding. Determination of heteronuclear $^{13}C,^1H$ coupling constants is especially helpful to determine the relative positions of the substituents on the 5-membered ring. The pyrrolidine ring will adopt a predominant conformation with the minimal steric hindrance due to the two isoclinal or equatorial 1′,2′,4′-groups (1′-methyl, 2′-carbonylamino-galacto-octopyranoside and 4′-propyl) (Fig. 1b). The vicinal $^3J_{1_H,1_H}$ and $^3J_{13_C,1_H}$ coupling constants are in good agreement with the calculated values (Table 3) for conformations, **P2** essentially (*envelope* $E_{4'}$ and *twist* $^{5'}T_{4'}$, *4′-endo* and *4′-endo*/*5′-exo*) and **P3** ($^{5'}$E), **P4** ($E_{1'}$ and $^{2'}T_{1'}$).

Conformation around the χ_1 C(5)–C(6) torsion angle. The $^3J_{1_H,1_H}$ and $^3J_{13_C,1_H}$ coupling constants are helpful to determine the position of the protons H(5), H(6) and at the same time, the orientation of the substituents (8-methyl and 4-pyranose groups).

The presence of the two bulkier substituents leads to a predominant *trans* conformation. Our observed NMR values ($^3J_{5,6}$, 9.7 Hz; $^3J_{C(4)H(6)}$ and $^3J_{C(7)H(5)}$, 1 Hz) (Table 3) should include an almost exclusive participation (≈90%) of the *t* conformation. A difference of 0.5 Hz compared with the calculated values, is not really larger than the experimental error (0.2–0.3 Hz).

Table 4. Qualitative nuclear Overhauser enhancement data and observed TRNOEs for lincomycin (**1**) and clindamycin (**2**) in D_2O buffered solution

	Lincomycin (**1**)		Clindamycin (**2**)	
^{1}H observed	NOEs[a]	TRNOEs[b]	NOEs[a]	TRNOEs[c]
1	SMe (m)	SMe (s)	SMe (m)	SMe (s)
2	1 (s)	SMe (w), 1 (s)	1 (m)	SMe (m), 1 (s)
3	1 (w), 2 (s)	2 (m)	1 (w), 2 (s)	1 (w), 2 (s)
4	1 (w), 2 (w), 3 (m)	3 (s)	3 (m)	SMe (w), 3 (m)
5	1 (w), 3 (m), 4 (s)	1 (w), SMe (m), 3 (s), 4 (m)	SMe (w), 1 (w), 2 (w), 3 (m), 4 (m)	SMe (m), 3 (m), 4 (s)
6	4 (w), 5 (s)	5 (s)	2 (w), 3 (w), 4 (w), 5 (s)	SMe (w), 4 (w)
7	6 (m)	6 (w), SMe (m)	5 (w), 6 (s)	SMe (m), 4 (w), 5 (m), 6 (s)
8	SMe (w), 5 (s), 6 (w), 7 (s)	SMe (w), 5 (s), 6 (w), 7 (m)	5 (w), 6 (m), 7 (m)	2 (w), 4 (w), 5 (w), 6 (s), 7 (s)
1′	4 (w)		4 (w)	4 (w)
2′	1′ (s)		1′ (m)	1′ (s)
3′a	2′ (m)		8 (w), 2′ (m)	1′ (m), 2′ (s)
3′b	8 (w), 2′ (m)	2′ (s)		
4′	3′a (m), 3′b (w)	3′ (s)	3′ (m)	2′ (s), 3′ (s)
5′a	4′ (m)	4′ (w)	3′ (w), 4′ (m),	1′ (m), 3′ (w), 4′ (m)
5′b	3′a (w), 4′ (w), 5′a (s)	4′ (w), 5′a (s)	4′ (w), 5′a (s)	2′ (m), 3′ (m), 4′ (m), 5′a (s)
1″	3′ (m), 4′ (m), 5′b (m)	3′ (w), 4′ (m), 5′a (w), 5′b (w)	3′ (s), 4′ (m), 5′a (w), 5′b (m)	1′ (m), 3′ (s), 4 ′(s), 5′a (m), 5′b (s)
2″	3′ (w), 4′ (m), 5′b (w), 1″ (s)	4′ (w), 1″ (w)	3′ (m), 4′(m), 5′a (m), 5′b (w), 1″ (s)	3′ (m), 4′ (m), 5′b (w), 1″ (s)
3″	4′ (w), 1″ (m), 2″ (s)	1″ (m), 2″ (s)	3′ (w), 4′(w), 5′a (w), 1″ (m), 2″(m)	3′ (w), 4′(w), 5′a (w), 1″ (m), 2″ (s)

[a]Observed ^{1}H NOE data from 2D ^{1}H NOESY ($\tau_m = 300$ ms, NOEs > 0); s = strong, m = medium, w = weak.
[b]TRNOESY (antibiotic/ribosome ratio = 1300, $\tau_m = 150$ ms, TRNOEs < 0) experiments in D_2O buffered solution at 293 K and pH = 7.6.
[c]TRNOESY (antibiotic/ribosome ratio = 625, $\tau_m = 150$ ms, TRNOEs < 0) experiments in D_2O buffered solution at 293 K and pH = 7.6.

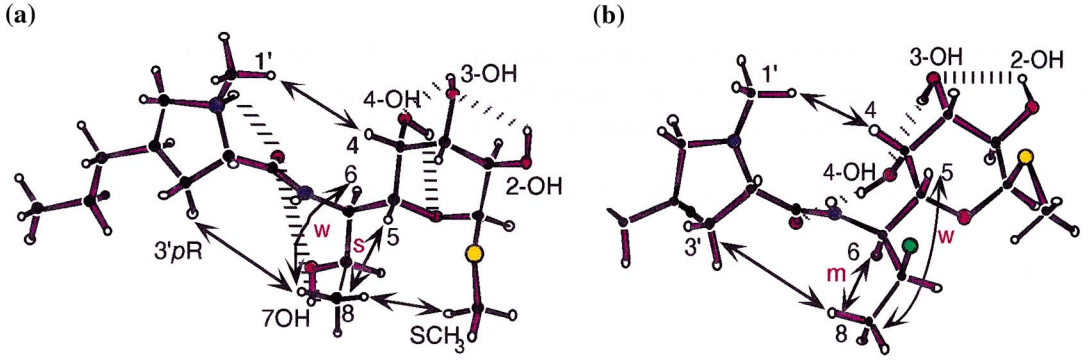

Figure 3. Some characteristic NOEs (< - >) and hydrogen bonding network (////) for (a) **G3** lincomycin (**1**) and (b) **G1** clindamycin (**2**) conformations.

Conformation of the χ_2 [C(6)–C(7)] torsion angle. The experimental coupling constants $^3J_{1_H,1_H}$ ($^3J_{6,7}$) and $^3J_{13_C,1_H}$ ($^3J_{C(5)H(7)}$, $^3J_{C(8)H(6)}$) presented in (Table 3) allow us to determine with tolerable precision the fractional populations of the three rotamers (Fig. 2a)- *Pt*, *Pg* and $(Pg)^+$. An estimate of the population of the *gauche* g^+ ($+60°$) conformation for lincomycin (**1**) was calculated to be 70±10% and similarly, for clindamycin (**2**) the population of the *trans t* (180°) staggered conformation was calculated to be 90±10%. Qualitative considerations may be also applied to distinguish the major rotamer. This may be accomplished using the heteronuclear $^3J_{N\text{-}H7}$ coupling constants of the rotamers about χ_2, strong for *trans t* rotamer or weak (and even invisible) for both g^+ and g^- rotamers (Fig. 2a). Thus, by an inverse ^{1}H, ^{15}N long range experiment, we have observed for **2** a large signal from the H(7) proton which is relative to a predominant conformations *t* about χ_2. In clindamycin (**2**), the electrostatic interactions (hydrogen bonding) are reduced, the preferred conformation is the sterically favoured *t* one. A similar experiment for **1** solution confirms that its major rotamer about χ_2 is the gauche one, g^+.

Considering the rotamer distribution relative to χ_1 and χ_2 (C(4)–C(5)–C(6)–C(7)–C(8)), the NMR study has demonstrated that their major species in aqueous solution are **G3** (t about χ_1 and g^+ about χ_2) for lincomycin (**1**) and **G1** (*t* about χ_1 and *t* about χ_2) for clindamycin (**2**), respectively (Fig. 2b). Furthermore these data will be confirmed by the molecular modelling study.

The NOEs observed for lincomycin (**1**), [6-H]4-H, [6-H]7-H and [5-H]8-Me can be compared to the theoretical distances, deduced from χ_1 and χ_2 rotamers, and then, all these observations may be rationalized by the presence of the **G3** *t* g^+ preferred conformation (Figs. 2b and 3). While the NOEs observed for clindamycin (**2**), [6-H]4-H, [6-H]7-H and [6-H]8-Me show the spatial proximity of the 6-H proton with both 7-H and 8-H (Fig. 3), and then, the presence of the **G1** '*tt*' preferred conformation was confirmed.

Conformation of the χ_3 (C(5)–C(6)–NH–CO) and χ_4 (C(3′)–C(2′)–CO–NH) torsion angles. From a 2D phase-sensitive ^{1}H NOESY experiment in DMSO performed with a mixing time, $\tau_m = 300$ ms, a strong interaction between N-H and 5-H reveals that these two protons are found '*cis*', relative to the amide bond plane (Fig. 1c). Moreover, the weak NOE between 6-H and N-H and the $^3J_{C(O)H(6)}$ and $^3J_{H(N)H(6)}$ coupling constants, 3 and 9 Hz, respectively (Table 3) allow us to conclude the 'extended' stereochemistry (Fig. 1c) of the amide bond (χ_3). Its orientation relative to the pyrrolidine ring, (χ_4) is confirmed by the strong NOE [N-H]2′-H (Table 4) which implies N-H and 2′-H eclipsed or O=C and 2′-H anti (Fig. 1c).

Carbon-13 spin-lattice relaxation times (T_1). T_1 values were used to probe the mobility of the protonated carbons in lincomycin (**1**) and clindamycin (**2**). Information about the structural flexibility of these compounds can be obtained experimentally from the T_1 relaxation times of the carbon resonances as the NT_1 values (N = number of attached protons, T_1 = longitudinal relaxation time) correlate directly with the molecular mobility.[33]

The similarity of the average NT_1 values for the pyranose ring carbons, <0.38 s$>$ and <0.40 s$>$ for **1** and **2**, respectively, indicates isotropical tumbling of this moiety without preferred axis of rotation. The motion of C(6) and C(7) is isotropic with the sugar ring as evidenced by the essentially identical average T_1 values with those of the pyranose methine carbons (<0.38 s$>$ and <0.37 s$>$ for **1** and **2**, respectively). Examination of these average T_1 values yields the following conclusion that no free rotation occurs around the C(6)/C(7) axis. This rigidity was noted in the conformational analysis with the predominant H(5) and H(6) *trans* and H(6) and H(7) *gauche* in both lincomycin and clindamycin. The pyrrolidine ring is characterized by an increased mobility with respect to the sugar moiety according to increased average NT_1 values (<0.59 s$>$ and <0.61 s$>$ for **1** and **2**, respectively). The NT_1 value for C(2′) is markedly lower (0.46 s for **1** and **2**, respectively) than the average NT_1 value of the pyrrolidine ring, suggesting that C(2′) is on a preferred axis of rotation. Important free rotation is experienced by the methyl groups [C(8)-Me, C(3″)-Me, N(1′)-Me and S(1)-Me] and the C(4′) side chain carbons [C(1″) and C(2″)]: the average NT_1 values of C-Me or C-propyl chain are higher than those of C-pyrrolidine, C-pyranose and C(6)–C(7).

The main difference between lincomycin (**1**) and clindamycin (**2**) in solution is shown by the shorter T_1 values of the Me(8) group ($\approx -40\%$) for **2** and may be associated with the presence of the heavy chlorine atom. The mobility of its (C(4)–C(5)–C(6)–C(7)–C(8)) fragment is reduced in agreement with the presence of the major **G1** conformer and accordingly to the observed $^3J_{5,6}$ and $^3J_{6,7}$ values. The Me(8) is thus pushed into a more sterically hindered environment. Consequently, the motion of the opposite side, i.e. the propyl chain is liberated in clindamycin and its NT_1 values were longer. This observation suggests that the end of the chain in clindamycin may fluctuate between relatively close positions, in good agreement with the absence of NOEs between Me(3″) and pyrrolidine ring protons.

Molecular modelling

It was important to compare the NMR results with those obtained from molecular modelling in order to characterize all the different conformations present in solution.

The structures of lincomycin (**1**) and clindamycin (**2**) obtained from the X-ray structures[34] were built with the software Insight II using DISCOVER program from the BIOSYM package. In addition to the 10 *envelopes*, the different (t, g^-, g^+) conformations existing for each torsion angle (χ_1, χ_2, χ_5 and χ_6) have to be considered. The amide bond between the galacto-octopyranoside ring and the propyl-pyrrolidinyl ring was fixed in the *trans* geometry. The side chain around χ_3 and χ_4 (Fig. 1c) is flexible and the structures coresponding to χ_3 dihedral angle value of $+140°$ which imply χ_4 dihedral angle values of $+140°$ or $+120°$ were more stable than those having χ_3 or χ_4 $\pm 60°$. The extended ($\pm 140°$) position of the amide bond (χ_3 and χ_4) was clearly determined by the NOESY experiment. A folded structure ($\pm 60°$) is only required in the intermediate "higher-energy" structures when an interconversion is observed between the two chair conformations of the pyranose ring.

The purpose of the molecular dynamics method was to examine the structural and dynamical behaviour of the system and to sample regions of conformational space that are not attainable using other computational procedures. A protocol was also performed with protonated **1** and **2** molecules by adding one formal charge (i.e. on the the 1′-amino group). To mimic the solvent effect, the relative permittivity was set to be distance-dependent, $\epsilon = 4R_{ij}$ in the description of the Coulombic interaction[35] in avoiding an explicit modelisation of water molecules. The results are summarized in Tables 5 and 6.

For a preliminary exploration of the conformational space, a MD run at 300 K with periodic temperature jumps to 600 K was performed to supply the system with energy (Table 5) and then, to allow high potential energy barriers separating interesting regions of conformational space to be crossed. However, the results cannot lead to a statistical evaluation of the different conformations which participate in the NMR solution. To find an optimal protocol for better sampling and statistical evaluation, a method of multiple starting points has to be considered just as the time of MD run.[36]

Starting from structures with the conformation **G1**–**G3** (Fig. 2a) of the galacto-octopyranoside, different *envelope* type of the pyrrolidine group (**P2**–**P4**), a variety of possibilities (**C1**–**C9**) for the propyl chain, the simulation was stopped every picosecond, and the remaining structure energy minimized. As can be seen in Table 5,

Table 5. Energy and torsion angles computed for structure families of lincomycin (**1**) and clindamycin (**2**) represented by 18 types of low energy conformations

Family	structure **S**		Conformation $\chi1,\chi2$[a]	*envelope*[b]	χ_5,χ_6[c]	Energy *E*p (Kcal mol^{-1}) (**1**)	(**2**)	(**1**) (Protonated)	(**2**) (Protonated)
I	S1	G1P1C1	*tt*	$^{3'}$E	*tt*		48.4		
		G1P1C7			tg^+		45.4		
	S2	G1P2C1	*tt*	$E_{4'}$	*tt*	41.4	42.7	49.0	52.6
		G1P2C2			tg^-	42.3	43.0	50.0	50.6
		G1P2C3			tg^+	44.7	44.0		
		G1P2C4			g^-t		45.3		
		G1P2C5			g^-g^-		47.4		
		G1P2C7			g^+t	41.3	42.0	48.9	49.6
		G1P2C8			g^+g^-	43.2		51.2	51.6
		G1P2C9			g^+g^+		43.0	49.7	50.6
	S3	G1P3C1	*tt*	$^{5'}$E	*tt*				50.4
		G1P3C7			g^+t			49.6	50.4
	S4	G1P5C4	*tt*	$^{2'}$E	g^-t		45.8		
		G1P5C7			g^+t	43.7		50.7	51.4
		G1P5C9			g^+g^+			51.8	52.4
	S5	G1P6C1	*tt*	$E_{3'}$	*tt*		45.4	51.2	51.9
		G1P6C2			tg^-	45.0		52.9	53.1
		G1P6C3			tg^+		47.0		
		G1P6C7			g^+t	43.4	44.1	50.7	51.5
		G1P6C8			g^+g^-	47.4			
		G1P6C9			g^+g^+			53.0	
II	S6	G2P1C7	tg^-	$^{3'}$E	g^+t	45.5			
	S7	G2P2C1	tg^-	$E_{4'}$	*tt*		45.1		
		G2P2C2			tg^-	42.7	46.1	50.3	53.4
		G2P2C7			g^+t	41.6	44.9	49.0	
		G2P2C8			g^+g^-	43.6		51.0	
		G2P2C9			g^+g^+	43.8		50.0	
	S8	G2P3C7	tg^-	$^{5'}$E	g^+t			50.0	
	S9	G2P4C7	tg^-	$E_{1'}$	g^+t			51.2	
		G2P4C9			g^+g^+	51.9			
	S10	G2P5C2	$tg-$	$^{2'}$E	tg^-			56.9	
		G2P5C5			g^-g^-		51.1		
		G2P5C7			g^+t			51.3	
		G2P5C9			g^+g^+			52.4	
	S11	G2P6C1	tg^-	$E_{3'}$	*tt*	44.6			
		G2P6C2			tg^-			54.8	
		G2P6C7			g^+t	43.7		50.9	
		G2P6C8			g^+g^-	46.5			
		G2P6C9			g^+g^+	45.8		55.2	
	S12	G2P7C7	tg^-	$^{4'}$E	g^+t	51.8			
		G2P7C9			g^+g^+	50.7			
III	S13	G3P1C7	tg^+	$^{3'}$E	g^+t		47.7		
		G3P1C9			g^+g^+		49.2		
	S14	G3P2C1	tg^+	$E_{4'}$	*tt*			49.2	
		G3P2C2			tg^-		44.6	50.1	
		G3P2C3			tg^+		46.2	51.1	
		G3P2C7			g^+t	41.4	43.5		51.2
		G3P2C8			g^+g^-				53.1
		G3P2C9			g^+g^+	42.4	46.2	50.2	
	S15	G3P3C1	tg^+	$^{5'}$E	*tt*	45.0			
		G3P3C7			g^+t		47.0		52.5
	S16	G3P4C7	tg^+	$E_{1'}$	g^+t				52.9
	S17	G3P5C7	tg^+	$^{2'}$E	g^+t				53.6
		G3P5C8			g^+g^-				55.1
		G3P5C9			g^+g^+			52.9	
	S18	G3P6C1	tg^+	$E_{3'}$	*tt*			51.5	
		G3P6C2			tg^-			52.2	
		G3P6C7			g^+t	44.4	45.6	51.0	53.0
		G3P6C9			g^+g^+	48.7			

[a]Torsion angles $\chi1$ (C(4)–C(5)–C(6)–C(7)) and χ_2 (C(5)–C(6)–C(7)–C(8)) for the galacto-octopyranoside.
[b]Envelope conformations of the propyl-pyrrolidinyl ring.
[c]Torsion angles χ_5 (C(3′)–C(4′)–C(1″)–C(2″)) and $\chi6$ (C(4′)-C(1″)-C(2″)-C(3″)) for the 1′-methyl-4′-propyl-proline fragment.

three conformational families ($\mathbf{S_I}$–$\mathbf{S_{III}}$) were found this time.

The main difference between lincomycin and clindamycin appeared here. The G1P2 ($\mathbf{S_I}$) structures from MD are more stable for clindamycin than the others, the necessary activation energy for this observed transitional event ('**G2**<->**G1**<->**G3**') was probably attained with difficulty in clindamycin solution.

The stability of the different conformers (Figs. 4 and 5) was tested by a 300 ps dynamics protocol at 300 K. The frequency (how many times we get the same conformation) was deduced from the different structures and the statistical evaluation will be done during this process. We have run six dynamics starting from $\mathbf{S_I}$–$\mathbf{S_{III}}$ protonated and unprotonated molecules which totalled a 3600 ps simulation, applying the distance constraints obtained from the NMR experiments.

Molecules **1** of lowest energies generated during this protocol are mainly of G3P2 (S14) conformation, involving both extended propyl chain conformations, 'C1' (35%) and 'C7' (25%) conformers. This $\mathbf{S_{III}}$–G3 conformation is stabilized by the hydrogen bonding 7-OH///O=C between the (C(5)–C(6)–C(7)–C(8)) moiety and the amide unit (Fig. 3a). It appears that this inter-residue hydrogen bonding plays a role in determining the conformation of a large region of the galacto-octopyranoside, i.e. the conformation **G1**–**G3** of the χ_1, χ_2 rotamers (Fig. 2b). G2P2C7 (S7) structure of higher energy ($\Delta E = +5$ kcal mol^{-1}) exhibits an inter-residue hydrogen bond 4-OH///O=C, the 7-hydroxyl moves above pyranose and pyrrolidine rings and this allows the free rotation around the C(6)–C(7) (χ_2) bond. This orientation of the 7-hydroxy group was particularly favoured in the protonated molecule when the NH of the pyrrolidine group (NH///O=C) disrupts the hydrogen bonding which occurred between OH(7) and CO. The lincomycin $\mathbf{S_I}$–G1 structure was not stable even during protocol at 300 K and it leads to the $\mathbf{S_{III}}$–G3 structure.

Clindamycin generated essentially $\mathbf{S_I}$–G1 family (53%) corresponding to G1P2C4 (33%) and C7 (20%) conformations (S2). The $\mathbf{S_{II}}$–G2 structure was not stable during the 300 K MD simulation performed with distances constraints based on the NOE data and an interconversion to $\mathbf{S_I}$–G1 was observed. The generated structures confirmed the tendency of the Cl atom to favour the '**G1**' orientation (Fig. 3b), the most stable one. The minor $\mathbf{S_{III}}$–G3 conformation (G3P2C7) corresponds to a S14 structure of "higher energy" (3 kcal above the minimum). The S14 structure leads to another C9 orientation of the propyl group relative to the pyrrolidine, (G3P2C9).

It is thus concluded, from NMR and MD data that lincomycin exists in aqueous solution (Fig. 4) as two major conformers, S7 (G2P2C7) and S14 (G3P2C1, C7) but it cannot adopt the $\mathbf{S_I}$–G1 conformation. On the other hand, the analogue clindamycin presents the major conformer, S2 (G1P2C4, C7) with the minor ones S14

Table 6. Lincomycin (**1**) and clindamycin (**2**) inter-proton distances from minimized structures derived from MD

Connectivities	Inter-proton distances[a]						
Intra-galacto-octopyranoside	**(1)-G1**	**(1)-G2**	**(1)-G3**	**(2)-G1**	**(2)-G2**	**(2)-G3**	
1-SMe	m	m	s	s	s	s	
5-SMe	s	m	m	m	s	m	
6-SMe	w		w	w	w	w	
7-SMe	s		s	s	s	m	
7-5	s	m	m	s	s	m	
7-4	w	w	w	w	w	w	
8Me-SMe	w	m	m	w	m	s	
8Me-2	w				w		
8Me-4			w			w	
8Me-5	w	s	m	w	m	s	
Intra-pyrrolidinyl	**P1** ($^{3'}$E)	**P2** ($E_{4'}$)	**P3** ($^{5'}$E)	**P4** ($E_{1'}$)	**P5** ($^{2'}$E)	**P6** ($E_{3'}$)	
5′a(*p*S)-1′Me	m	s	s	s	m	m	
5′a(*p*S)-3′	s	m	s, m	m, w	m	s, m	
5′b(*p*R)-2′	w	w	m	s	m	m	
5′b(*p*R)-3′	m	m (3′*p*R)	m (3′*p*R)	m	m	m (3′*p*R)	
5′b(*p*R)-3′a(*p*S)	w	w	w	m	m	w	
Pyrrolidinyl-galactose							
1′Me-4	m	m			w	s	
3′a(*p*S)-8Me	m				w	m	
3′b(*p*R)-8Me	w	w			m	w	
Propyl chain -pyrrolidinyl	**C1** (*tt*)	**C2** (*tg*−)	**C3** (*tg*+)	**C4** (*g*−*t*)	**C7** (*g*+*t*)	**C8** (*g*+*g*−)	**C9** (*g*+*g*+)[b]
1″-1′Me	w	w	w				
1″-3′	m	s	s, m	s	s	m, s	s
1″-4′	m	m	m	s	s	s	s
1″-5′a(*p*S)	s	m	s	m	m	m	m
1″-5′b(*p*R)	m	s	m	m	m	m	m
2″-3′	w	s	w		s	s	m
2″-5′a(*p*S)	s	w	s	m	m	s	m
2″-5′b(*p*R)	s	w	s	m	m	m	m
3″Me-3′		m	w	w	w	s	w
3″Me-4′	w	w	m	w	w	w	w
3″Me-5′a(*p*S)	w	w	w	w	w	w	m

[a]Some evident intra-unit contacts found for the different structures are not specified. 2–3 Å, s: strong, 3–4 Å, m: medium, 4–5 Å, w: weak.
[b]Only for clindamycin.

(G3P2C7, C9) (Fig. 5). The major **G3** and **G1** conformations are favoured for **1** and **2**, respectively and the calculated populations of rotamers are in a good agreement with the NMR experimental data.

The similarity between an averaged geometry in solution and several MD conformers was investigated from the experimental (NMR) coupling constant values and the intensive NOESY correlations observed. For each conformation obtained from this protocol, coupling constants $^3J_{H,H}$ and $^3J_{C,H}$ are calculated and are compared to the observed vicinal coupling constants (Table 3). The spatial proximity values computed from the low-energy structures in different conformations (Table 6) were also compared with the observed NOE values.

By using *Pi*, the fractional population for each *i*th conformational microstate, the average coupling constant can be computed from: $^3J_{(HH)} = \Sigma Pi * {}^3Ji_{(HH)}$ and $^3J_{(HC)} = \Sigma\ Pi * {}^3Ji_{(HC)}$

Experimental values were compared to the calculated values from the conformational equilibrium generated by the summed MD trajectories (Figs 4 and 5) and a good correlation was found.

The $\Sigma\ \Delta(J_{calc} - J_{exp})$ evaluated from about 25 coupling constants ($J_{H,H}$ and $J_{C,H}$) lead to an average value ($< \Delta > \pm 1.4$ Hz). The fit between MD data and the experimental NMR ones show that solution averaging (Figs 4 and 5) is well described and conformational space well sampled (the small difference is attributed to a slight variation of the minor conformers).[37] The structures achieved by MD (Figs 4 and 5) will be taken into account for representing the compounds as every one can be in relation to the active site.

Structural characteristics of lincosamides bound to bacterial ribosomes

We studied lincosamide-ribosome interactions to *E. coli* ribosomes, using two-dimensional transferred nuclear

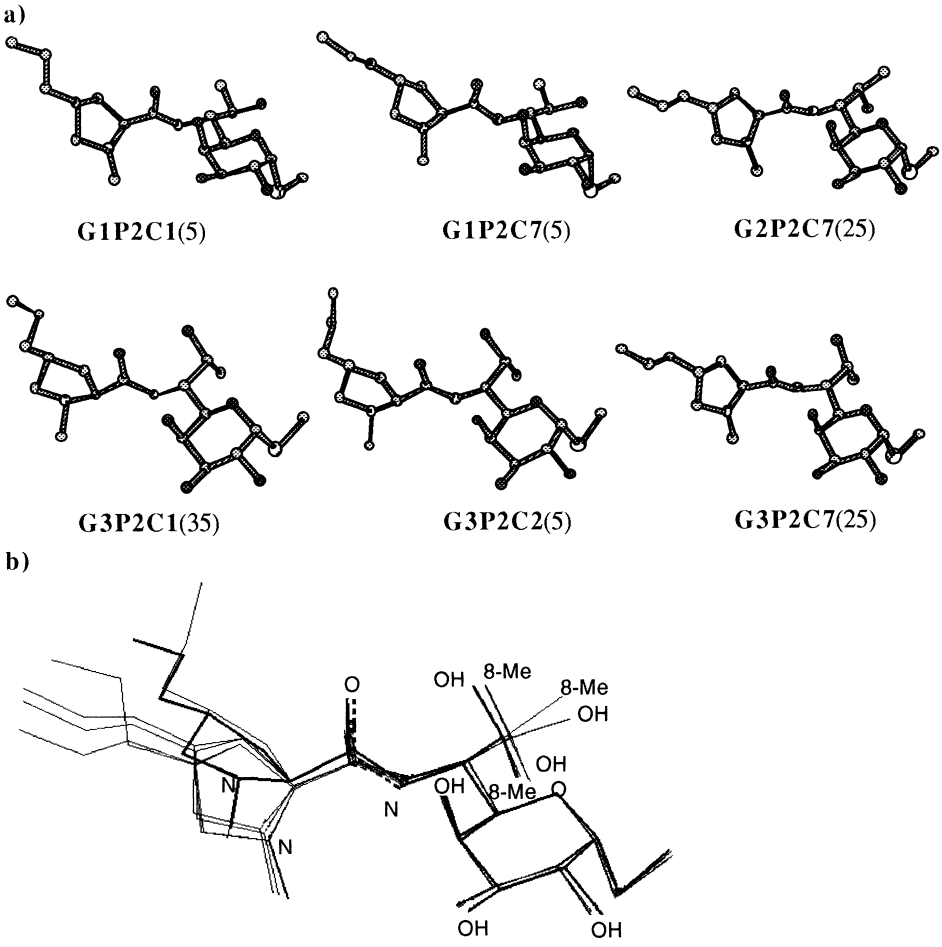

Figure 4. (a) Lowest energy structures of lincomycin (**1**) generated by MD with distances constraints based on the observed NOE data. (b) Superimposition of these structures to represent **1** conformational averaging in solution.

Overhauser effect spectroscopy (TRNOESY).[12,19–21] The information present in TRNOE analysis focuses on a plausible conformation essential for the drug's antibacterial action when binding to the bacterial ribosome.

Physical parameters of crucial importance for the chemical exchange such as temperature, ligand-ribosome ratio and *E. coli* ribosomal concentration have to be optimized in order to develop the TRNOESY experiment in the specific case of the lincosamide–ribosome interaction.[12]

Room temperature seemed better for fast exchange upon complex formation and led to optimal conditions for the TRNOESY experiment. The samples of **1** and **2** were dissolved in an aqueous NaD_2PO_4/Na_2DPO_4 buffer (0.05 M) with KCl (0.2 M). Another parameter had to be refined, the TRNOEs time dependence of lincosamide antibiotics: $\tau_m = 300–500$ ms for lincomycin; likewise, spin diffusion effects appeared for mixing times larger than 150 ms for clindamycin.

Lincosamide/ribosome ratio. The line-broadening of lincosamides was proportional to the amount of ribosome. Transferred NOE effects from clindamycin–ribosome interactions could be observed with a 5000 ligand/ribosome ratio, as for the 14-membered macrolides. A concentration of 0.8 μM of *E. coli* MRE 600 strain 70S ribosomes with 4 mM of clindamycin was appropriate because it gave a significant increase of the line width of clindamycin (**2**). With this concentration of ribosomes, the line-broadening was then too weak to be detected for lincomycin (**1**). High ribosomal concentration (4 μM) with 2 mM ligand caused half line-broadening of the lincomycin signals as well as TRNOE clearly observable cross-peaks. Here, with a 500 ligand/ribosome ratio (like for josamycin and spiramycin),[16,38] transferred NOE effects from lincomycin–ribosome interactions could be observed only with such concentrations. These results suggested that lincomycin exhibited lower affinity for weak ribosomal interaction than clindamycin and the 14-membered macrolides previously studied.[11,12,39]

Bound conformation. The bound structure of lincosamides is blocked into specific and privileged conformations in weak interaction with *E. coli* ribosomes. In particular, NOEs relative to the **G1P2C2** conformation of clindamycin appear strongly with ribosomes.

MD simulations with distance constraints. From the TRNOE-distance constraints, the bound conformations were calculated. They could indicate the specific structural

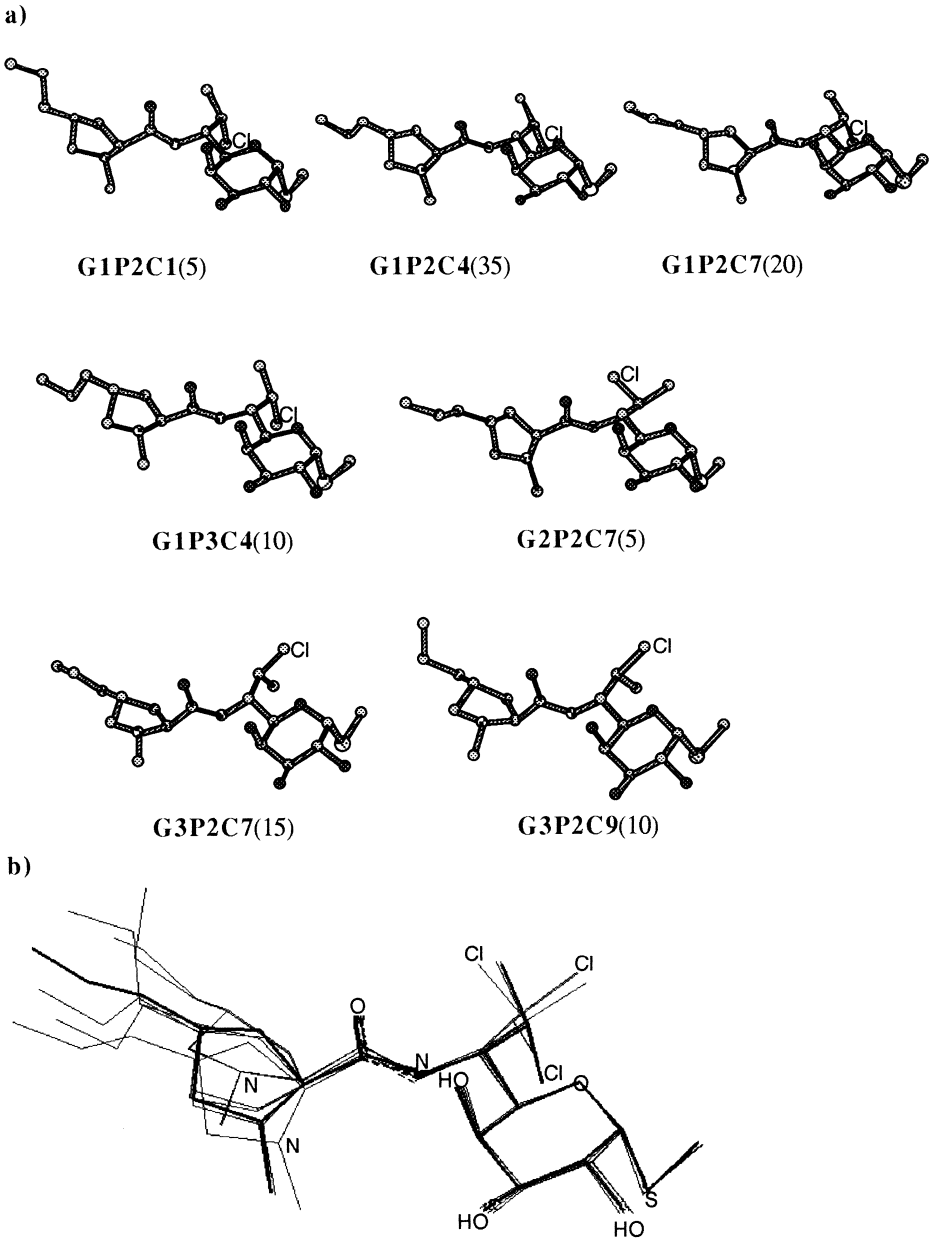

Figure 5. (a) Lowest energy structures of clindamycin (**2**) generated by MD with distances constraints based on the observed NOE data. (b) Superimposition of these structures to represent **2** conformational averaging in solution.

requirements of the weak binding receptor. The distances defined from the relative TRNOESY cross-peak intensities were set as follows: 2–3 Å (s), 3–4 Å (m) and 4–5 Å (w). Distances including methyl protons were referred to a pseudo-atom located at the center of the three methyl protons.[40] The quality of the resulting structures was evaluated by the average distance error $\{1/N\ \Sigma\ [d_{set}(i)–d_{model}(i)]$ where N is the number of constraints and d_{set} and d_{model} correspond to the distance from the constraint set and to the distance calculated from the generated conformation, respectively$\}$.

After dynamics protocol with TRNOE-distance constraints (300 ps MD run at 300 K) starting from ($\mathbf{S_I}$–G1, $\mathbf{S_{II}}$–G2 and $\mathbf{S_{III}}$–G3) protonated and unprotonated structures, the low energy structures are shown in Figures 6 and 7, respectively for lincomycin (**1**): **S7**–G2P2C1 (30%), **S14**–G3P2C1,C2 (60%) and for clindamycin (**2**): **S2**–G1P2C2 (65%), **S14**–G3P2C2 (35%).

The possible alternatives are that either lincomycin (**1**) and clindamycin (**2**) bind directly to the receptor with their major TRNOE conformations, then 7(*R*)-Cl and 7(*S*)-OH epimers bind differently on the same receptor site or if the minor ones are the active structures, conformational changes are involved for interacting with the receptor in multistep kinetics ($\mathbf{S_{III}}$–G3- > $\mathbf{S_{II}}$–G2 for **1** and $\mathbf{S_I}$–G1- > $\mathbf{S_{III}}$–G3 for **2**).

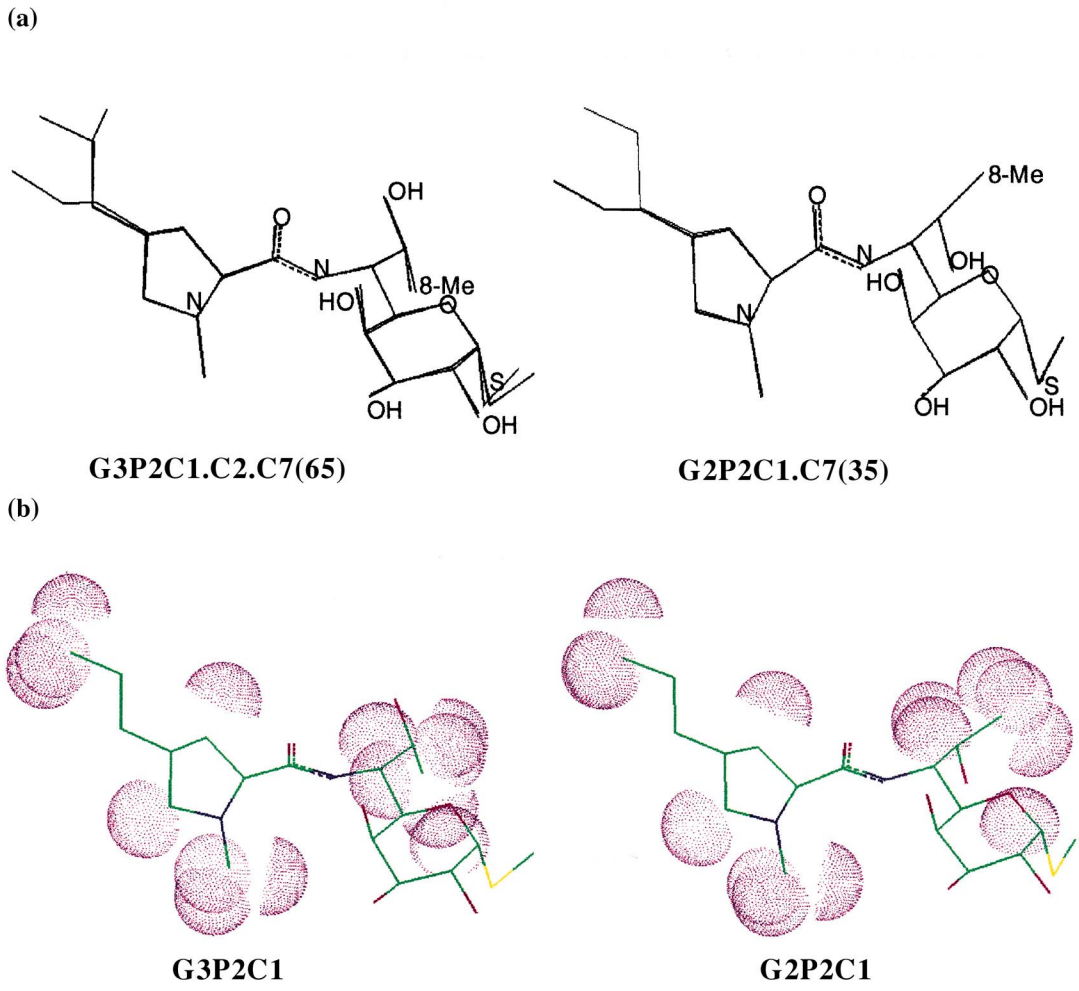

Figure 6. (a) Superimposition of the conformations **G3P2C1**, **C2**, **C7** (65%) and **G2P2C1**, **C7** (35%) generated by MD with distances constraints based on the observed TRNOE data for lincomycin (**1**). (b) Van der Waals' surfaces of the atoms whose signals are most broadened (5′b-H, 3′b-H, 2-H, 6-H, 7-H, 8-Me and 1′-Me) in the **G3P2C1** and **G2P2C1** bound structures to ribosomes. The broadening observed may reflect proximity to a binding surface.

Comparison of free and bound conformations. The bound conformation to the ribosome will be either the major conformation populated in solution (**2**-G1, **1**-G3) or a minor one of higher energy (**1**-G2). The TRNOE experiments suggest that clindamycin binds in the receptor site in essentially a similar conformation to its predominant one that exists free in aqueous solution (Fig. 7a). The TRNOESY spectra of clindamycin contain most of the crosspeaks which were due to hydrogens spatially proximate in the free drug. The bound structure shows a slight distortion of the propyl chain conformation in a structure **S2** such as 3″-Me ends spatially proximate to 8-Me. Stabilization of a sugar side chain conformation with a bulky group (8-Me) *trans* to the amide unit like it appears in **2**-G3P2C2 (Fig. 7a) seems to be sterically unfavorable for an interaction at the receptor.

It is clear that in lincomycin the existence of hydrogen bonding which occurred in free **1** between OH(7) and CO favours the major **G3** conformer in solution (Fig. 3). In the bound structure, the OH(7) may be potentially accessible to the binding site, and this allows the 8-methyl group, the pyrrolidinyl ring and the alkyl-side chain to occupy a less sterically congested environment in the **G2** rotamer. These modifications may be of importance for the lincosamide mode of action.

Comparison of 1 and 2 bound conformations. From these experiments, the **S2**-G1P2C2 conformation appears to be the clindamycin structure involved in weak specific binding to the bacterial ribosome (Fig. 7). Superimposition of the **1** (G2P2C1) and **2** (G1P2C2) bound structures (Fig. 8) shows that the unprotonated form (**G2**) of lincomycin places OH in the same spatial location as Cl in clindamycin (**G1**). Indeed, the structure representing the bound state of clindamycin shows conformational homology with the bound **S7**-G2P2C1 rather than the **S14**–G3P2C1,C2) conformation of lincomycin, after superimposition (Fig. 8), except in the Me(8) and Me(3″) regions. This is of particular interest since it could be related to the different biological properties of these molecules. Previous studies[22] on action of lincomycin and clindamycin have postulated a hypothesis about the conformational requirement of lincosamide ribosome target that it was interesting to strengthen. Considering the interaction between lincosamide and ribosome, the different groups, namely the

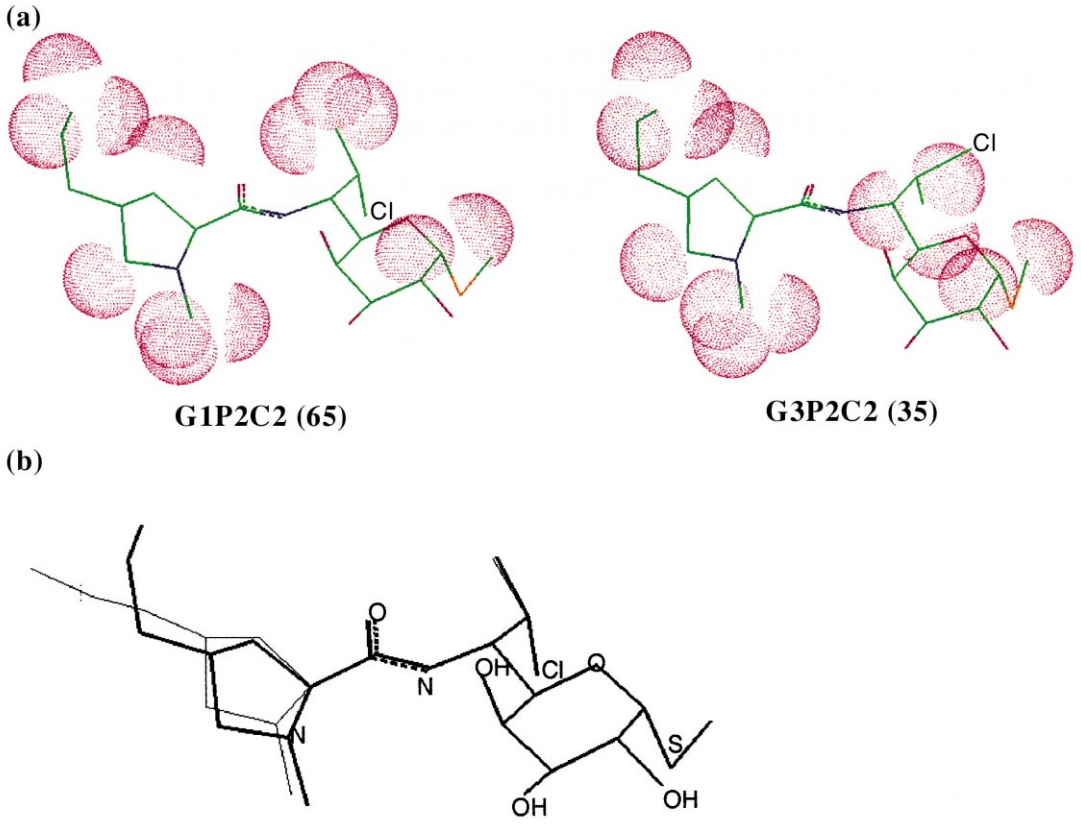

Figure 7. (a) Conformations **G1P2C2** (65%) and **G3P2C2** (35%) generated by MD with distances constraints based on the observed TRNOE data for clindamycin (**2**). The van der Waals' surfaces are shown to indicate the atoms whose signals are most broadened (3′b-H, 5′b-H, 1-H, 8-Me, 2-H, 1′-Me and 3″-Me) in the bound structures to ribosomes. (b) Superimposition of the free major **G1P2C7** conformation of clindamycin (**2**) in solution with its TRNOESY derived **G1P2C2** structure weakly bound to bacterial ribosomes, in bold.

alkyl substituents at the N′ atom and at the C-4′ in the pyrrolidine nucleus, the halogen substitution of the 7-(*S*) configuration of lincomycin molecule, the 8-Me group should be adequately arranged to favorably fit into the receptor.

After a superimposition procedure (Fig. 8), three main structural differences appear between lincomycin and clindamycin, **2** which is 20 times more active than **1**. (i) Firstly, the major conformation (**S14**–G3P2) of free lincomycin does not present the same structural analogy to the structure relevant to the receptor binding conformations (**S7**–G2P2) while for clindamycin, its major free conformation in solution corresponds mainly to the bound one (Fig. 7a). The biological activity of lincosamide antibiotics depends on many factors, and these may include their conformation in solution. The potencies of the lincosamide interactions with the ribosome binding site should be at least partially dependent on the relative abundance of each lincosamide conformation. (ii) Secondly, there is no overlapping of the 8-Me and 3″-Me groups in the two bound **1** and **2** structures. The 7-C configuration and the 4′-propyl-pyrrolidine chain should play a role in arranging respectively, the spatial position of the 8-Me and 3″-Me groups in the clindamycin molecule, for a good fit at the active site. (iii) Finally, the relative concentrations of unprotonated molecules could partially account for the relative activities of these drugs.[41] When comparing the two analogues, the relative stabilities of the protonated and unprotonated species could be affected by the difference in pK_a between clindamycin (7.3) and lincomycin (7.6). If the uncharged molecule is required for antibacterial activity,[22] clindamycin should reach the receptor site in greater concentration than lincomycin. Moreover, in the unprotonated lincomycin structure, the carbonyl is implicated in hydrogen bonding with 7-OH (with 1′-NH in protonated structure). On the other hand, when 7-OH is implicated in hydrogen bonding, this favors a different conformation (**G3**) than the plausible **1** conformation (**G2**) weakly bound to the bacterial ribosomes.

Binding surface. In general, a correlation between line broadening and involvement in binding is expected. A model of clindamycin showing the hydrogen atoms giving the most extensively broadened resonances was constructed (Figs 6b and 7a) using van der Waals' surfaces. The 'surface' of lincosamide deduced from the variation in line broadening would be indicative of the relatively rigid part of the molecule. The data corresponding to the pyrrolidine and the methyl (8-Me and 3″-Me) regions are indicative of near-rigid rotation of these atoms in close proximity to the ribosome due either to sterically hindered rotation or to specific interunit (ribosome-lincosamide) bonds involving this region.

(i) The broadening observed from the bound structure relative to this weak specific binding to the bacterial

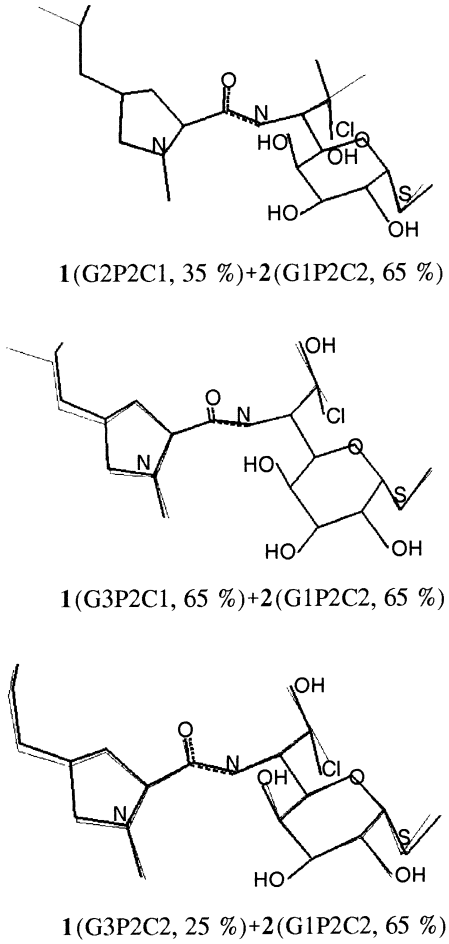

Figure 8. Superimposition of the major (65%) clindamycin TRNOESY derived **G1P2C2** structure with the lincomycin TRNOESY derived structures **G2P2C1** (35%), **G3P2C1** (65%) and **G3P2C2** (25%), respectively.

ribosome in the C(5)–C(6)–N(H)–C(O)–C(2′), C(3′)–C(5′) and 3″-Me, 8-Me region may reflect proximity to a binding surface.

The model was compared (Figs. 9 and 10) to the binding surface suggested for ketolides and for macrolides.[11,12,39] Macrolides bind to ribosomes at an identical 'surface', involving the C(13)–C(5) lactone region of the aglycone and both sugar rings, essentially the cladinose. The structures representing the bound state of the drugs (ketolide and roxithromycin)[39] show conformational homology after superimposition: the C(13)–O(1)–C(1) region is almost completely superimposable with variation in the 'right hand' side of the molecule, a stretching out of the desosamine dimethylamino group. In lincosamides, the propyl chain, the pyrrolidine, the fragments N(H)–C(O) and C(6)–C(8) and the 3″-Me spatially proximate to the 8-Me, all correspond to the macrocycle external part close to the 1-CO–3-CO region of macrolides (Fig. 10). Superimposition of the macrolide C(12)–C(15)–O(1)–C(1)–C(2)–C(5) region with the lincosamide C(5)–C(6)–N(H)–C(O)–C(2′) region of the bound structures revealed one change that may be of importance for the lincosamide mode of action. Lincomycin has the 8-Me in a different spatial location (Fig. 9) compared to 8-Me in clindamycin or 15-Me in other drugs (Fig. 10).

(ii) It was interesting to compare the line broadening of the galactose fragment in the lincosamides weakly bound to ribosomes to the line broadening affecting the cladinose sugar of macrolides in macrolide-ribosome complex. The broadened resonances of cladinose unit were supposed to indicate a steric hindrance of this residue in macrolide–ribosome complex since when it was removed in ketolides, the weakly bound state was strengthened. The superimposition in Figure 9b shows that the hindrance in this region tends to lessen with the galactose unit in clindamycin.

Drug-ribosome interaction. The weak Mg^{2+} independent interaction observed for macrolides (roxithromycin) and ketolides (HMR 3647) by NMR could be involved in the first step of recognition and selection of macrolide antibiotics by the ribosomal machinery with the second one being the strong interaction[13–15] responsible for the protein biosynthesis inhibition.[19] Compounds which are not able to take part in a weak binding interaction with bacterial ribosomes do not exert antibiotic activity, as also observed by Barber et al.[19,42] Thus, the weak binding seems to be a necessary step for the strong interaction.

The dissociation constant for strong lincosamide binding interaction with *E. coli* could not be measured by equilibrium dialysis and thus it was calculated in the range of 10^{-5} M.[4] This value is in the range which can be detected by NMR spectroscopy (10^{-3}–10^{-5}). Consequently, we could mistake the strong interaction for the low affinity characterized by transferred NOESY experiments since lincosamide 'tight' interaction being a faster exchange on the NMR time scale than for previously studied antibiotics. The equilibrium binding constant K_d related to the low affinity preinhibition binding site has been determined by direct NMR measurements of the dissociation constant (K_d) for antibiotic-ribosomes complex, using the T_2 (CPMG) and line-broadening methods.[43] The values of K_d with *E. coli* ribosomes were estimated in the range of 5.0 10^{-3}, 1.1 10^{-3} and 7.1 10^{-4} M, for clindamycin, roxithromycin and ketolide HMR 3647, respectively.

Then, the weak binding observed by TRNOE experiments is in agreement with a hypothesis of two distinct binding levels, as was reported for ribosome-tetracycline interaction,[44] with a low affinity binding level and the tight inhibition binding one. The fact that erythromycin resistance is not necessarily associated with lincomycin resistance favors the model that erythromycin and lincomycin act on different sites which could overlap.[45]

Conclusions

A combination of NMR spectroscopy and molecular modelling techniques showed that the major clindamycin solution state conformation is a 7-Cl '**G1**' type with respect to the presence of the heavy chlorine atom

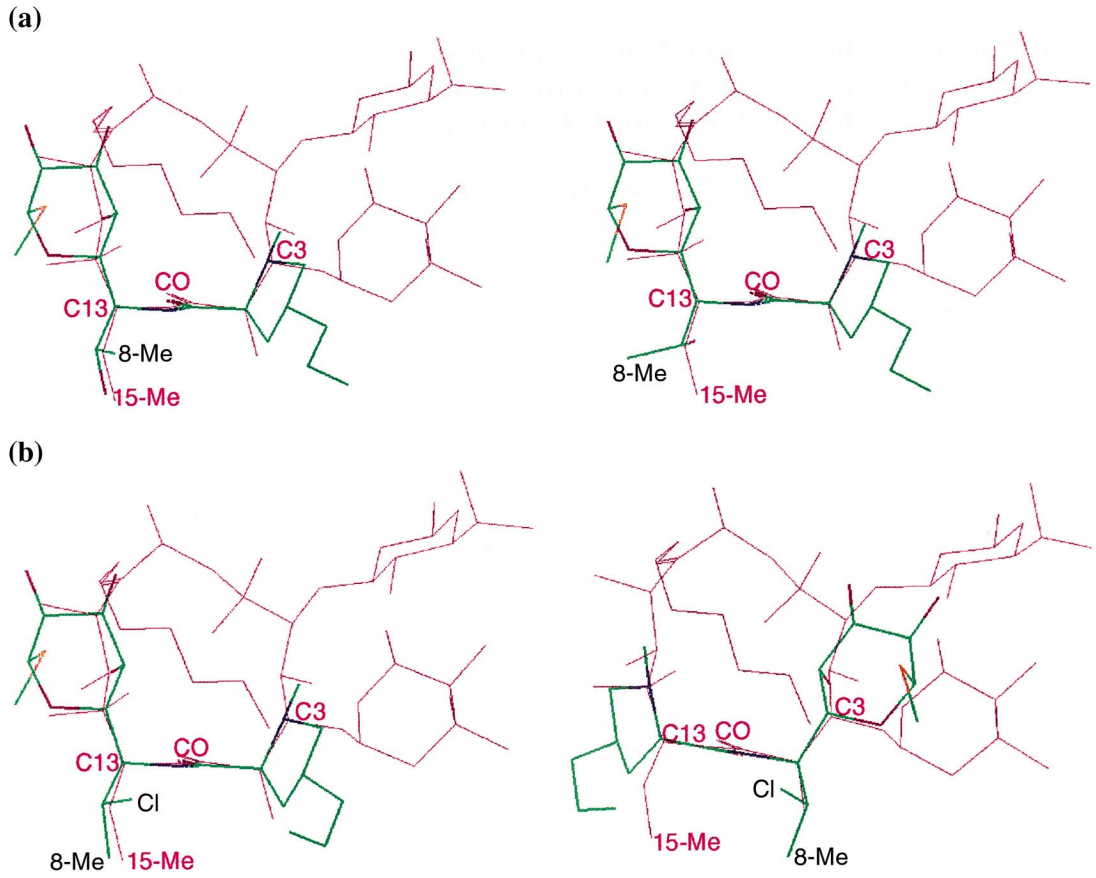

Figure 9. (a) Superimposition of the bound conformation of macrolide, roxithromycin with the major **G3P2C1** (65%) and the minor **G2P2C1** (35%) lincomycin TRNOESY derived structure, respectively. Quality of superimposition was evaluated by mean square (rms) deviation between the atoms (rms, 0.16 Å). (b) Two different types of superimposition (with a turn back of 180°) of the major **G1P2C2** (65%) clindamycin TRNOESY derived structure with the roxithromycin TRNOESY derived structure, (rms, 0.13 and 0.15 Å, respectively).

[**G1P2C7** (S2)], while the contribution of the 7-OH '**G3′** conformer in the lincomycin solution increases as the 7-OH is implicated in a hydrogen bond with the carbonyl of the amide group [**G3P2C1** (S14)].

Here also, TRNOE NMR experiments proved to be efficient for the location and detection of the weak interactions due to ribosomal activity providing a relationship between conformation in interaction and activity. These results can explain some of the differences observed between clindamycin and lincomycin and 14-membered macrolides (larger ratio). Thus, clindamycin exhibits higher affinity for weak ribosomal interaction than lincomycin.

In conclusion, the bioactive macrolide, ketolide and lincosamide (clindamycin) antibiotics studied displayed a strong NMR response. It is hence reasonable to suggest that TRNOE NMR experiments could describe binding sites present on ribosomes important in the inhibition process of antibiotics.

The superimposition of the C(6)–C(2′) ribosomal binding region of lincosamides with the south part C(2)–C(13) of the macrolactone ring displays conformational similarities. This is of particular interest since it could be related to the biological properties of these molecules as competitive inhibition occurs between the various MLS drugs.[46] This study shows that these antibiotics likely share a common ribosomal binding surface since it is possible to relate C(3), C(4), C(5), C(6), C(7), C(Me8), N(H), C(O), C(2′) and N(1′) in clindamycin with C(10), C(11), C(12), C(13), C(14), C(Me15), O(14), C(O), C(2) and C(3) in macrolides or in ketolides (Fig. 10). The conformation of this fragment seems to be crucial for the antibiotic-ribosome recognition site and it would be a plausible pharmacophore.

Experimental

NMR spectroscopy

The antibiotic samples were dissolved in an aqueous NaD_2PO_4/Na_2DPO_4 buffer (0.05 M), with KCl (0.2 M) at physiological apparent pH 7.6 (pD = pH + 0.4, uncorrected here) and it was possible to attain concentrations of 4 mM for ^1H experiments. The high K^+ concentration (200 mM) was used for better ribosome stability. A crystal of $TSPD_4$, 3-(trimethylsilyl) [2,2,3,3-d_4] propionic acid, sodium salt, was used as internal reference for the proton shifts. The errors on the chemical

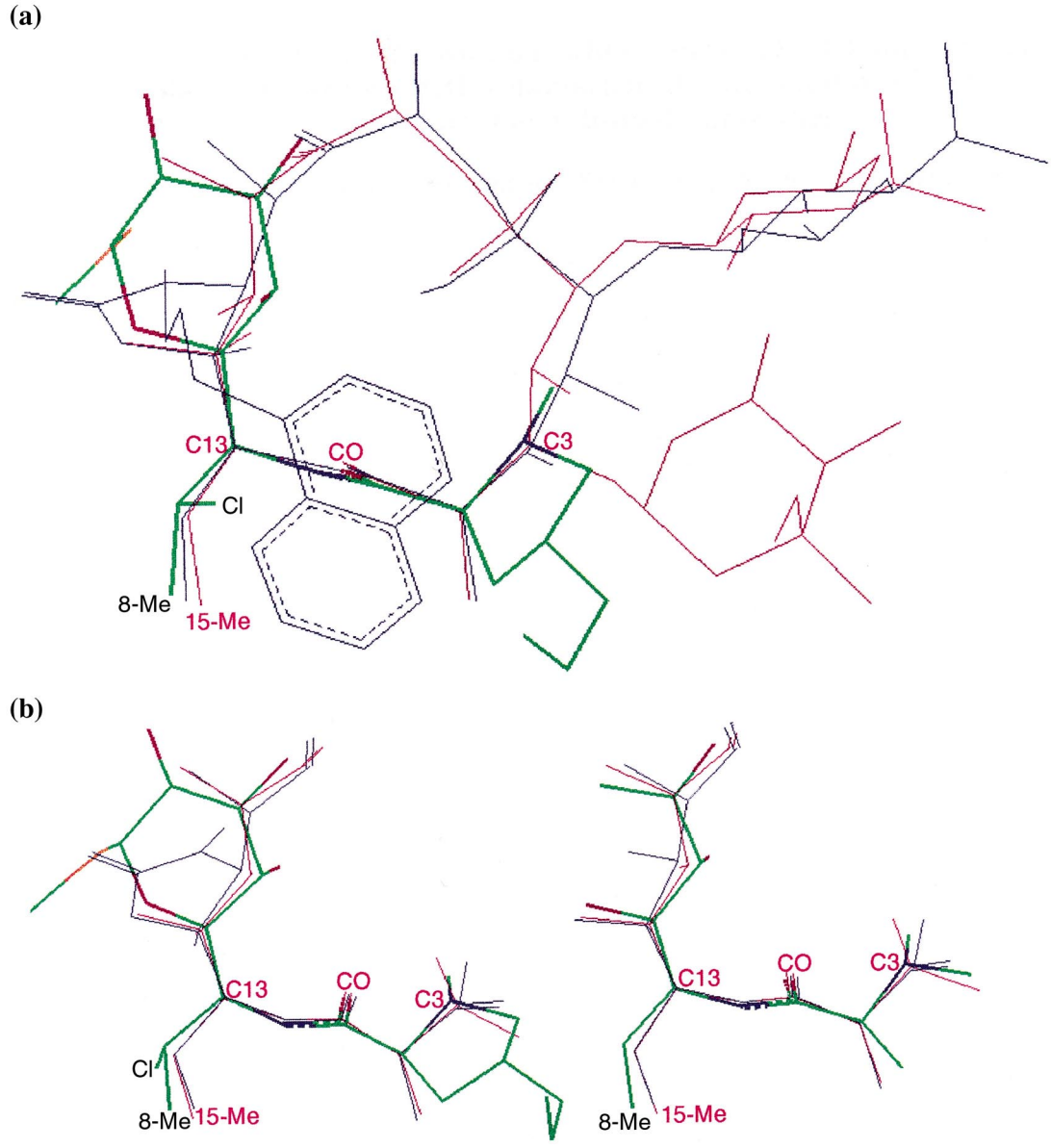

Figure 10. (a) Superimposition of lincosamide (clindamycin), ketolide (RU004) and macrolide (erythromycin) TRNOESY derived structures, weakly bound to bacterial ribosomes. It is possible to relate C(3), C(4), C(5), C(6), C(7), C(Me8), N(H), C(O), C(2′) and N(1′) in clindamycin with C(10), C(11), C(12), C(13), C(14), C(Me15), O(14), C(O), C(2) and C(3) in macrolides and ketolides. (b) The common fragment corresponding to the superimposition of the C(6)–C(2′) region of lincosamides with the south part C(2)–C(13) of macrolides and ketolides displays conformational similarities, e.g., the central atoms of the functional groups: the amide CO and α-N (lincosamides) with the ester CO and α-O (macrolides and ketolides).

shifts are 0.01 ppm for ^{1}H. The experiments were run at 500 MHz for ^{1}H, at 293 K, on Bruker AMX 500 Spectrometers equipped with a Silicon Graphics workstation. A presaturation of the solvent was used for all the 1D and 2D ^{1}H experiments.

The inverse correlation ^{1}H, ^{13}C- and ^{1}H, ^{15}N-HMBC experiments (PFG-HMBC, Pulse Field Gradient-Heteronuclear Multiple-Bond Correlation) were recorded at 293 K using a transfer delay of 80 ms (^{13}C) or 50 ms (^{15}N), with 256 experiments of 1024 data points, a sweep width of 3876 Hz in f_2 and 26,412 Hz (^{13}C) or 20,275 Hz (^{15}N) in f_1. One millisecond half-sinusoid gradients of 20, 20, and 10 G/cm (^{13}C) or 20, 10, and 6.95 G/cm (^{15}N) were used to select protons attached to carbon and the delay of 80 ms (^{13}C) or 50 ms (^{15}N) which was optimum for two- or three-bond couplings (delay = 1/2 $^{3}J_{X\text{-}H}$ delay). The 90° non-selective proton pulses were 9.5 μs long while the 90° non-selective carbon or azote was 10.5 or 20 μs, respectively. A low pass J filter was used with a value of 3.5 ms for the $\Delta = 1/2\ J_{C\text{-}H}$ delay optimum to remove $^{1}J_{C\text{-}H}$ connectivity. To carry out the gradient-selected J-HMBC experiment, eighteen 2D spectra were acquired with 256 t_1 increments and 32 scans per increment for $\tau_{max} = 200$ ms resulting in a total measuring time of 54 h. The 180° X-pulse during τ_{max} is a $90°_{x}$-$180°_{y}$–$90°_{x}$ composite pulse.

The 2D phase-sensitive using States-TPPI method ^{1}H TRNOESY experiments in D_2O buffered solution were performed using a mixing time of 150 ms. FIDs were acquired (32 scans) over 5555 Hz into a 2K data block for 256 incremental values of the evolution time and a relaxation delay of 2 s. Water suppression was performed

by a low power transmitter pulse of presaturation (70 dB) during relaxation delay and mixing time. One half-sinusoid (5% truncated) shape homospoil gradients of 10 G/cm were used during mixing time.

Molecular modelling

The calculations were run on a silicon-graphics computer using the Biosym software 'INSIGHT II' and 'DISCOVER' with the CVFF Forcefield.[47] Three different starting conformations (G1, G2 and G3) of lincomycin (**1**) and clindamycin (**2**) and TRNOESY data were applied. The dynamics were run for 300 ps (constant temperature). The trajectory was sampled by minimizing and storing the structure every picosecond.

The structures were built from the crystallographic coordinates of **2** as a starting point. Their atomic potentials and charges were recalculated using the built-in algorithm of the program[48] and the structures were modified into protonated molecules as they are bound to the bacterial ribosome at physiological pH 7.6. In order to take account of the polarization state due to protonation of the N′ atom of the pyrrolidine nucleus, the charges were recalculated[49] using the DISCOVER algorithm, with a total charge of +1. All calculations were performed implicitly taking account of the solvent, using in the description of the coulombic interaction a distance-dependent dielectric constant ($\epsilon = 4r$). After energy minimization and an equilibration period of 6 ps, a 50 ps MD run was performed at 300 K with periodic temperature jumps to 600 K. The 50 ps trajectory was sampled every picosecond and the remaining structures were then minimized by molecular mechanics and stored. The final conformers with lowest energies were then further minimized to a gradient less than 0.01 kcal/mol to obtain their energies at higher accuracy.

The three minimized conformations (G1, G2 and G3) were then used as starting structures of both lincosamides for a 300 ps MD run and NOESY or TRNOESY data were applied. Conformational similarities were evaluated using a superimposition procedure and by calculating the RMS of deviation between heavy atoms for each possible pair of the different structures.

References

1. Hoeksema, H.; Bannister, B.; Birkenmeyer, R. D.; Kagan, F.; Magerlein, B. J.; MacKellar, F. A.; Schroeder, W.; Slomp, G.; Herr, R. R. *J. Am. Chem. Soc.* **1964**, *86*, 4223.
2. Birkenmeyer, R. D.; Kagan, F. *J. Med. Chem.* **1970**, *13*, 616.
3. Campbell, J. M.; Reusser, F.; Caskey, C. T. *Biochem. Biophys. Res. Commun.* **1979**, *90*, 1032.
4. Douthwaite, S. *Nucl. Acids Res.* **1992**, *20*, 4717.
5. Vannuffel, P.; Di Giambattista, M.; Morgan, E. A.; Cocito, C. *J. Biol. Chem.* **1992**, *267*, 8377.
6. Vannuffel, P.; Cocito, C. *Drugs* **1996**, *51* (Suppl. 1), 20.
7. Di Giambattista, M.; Engelborghs, Y.; Nyssen, E.; Cocito, C. *J. Biol. Chem.* **1987**, *262*, 8591.
8. Arevalo, M. A.; Tejedor, F.; Polo, F.; Ballesta, J. P. G. *J. Biol. Chem.* **1988**, *263*, 58.
9. Di Giambattista, M.; Nyssen, E.; Pecher, A.; Cocito, C. *Biochemistry* **1990**, *29*, 9203.
10. Tejedor, F.; Ballesta, J. P. G. *Biochemistry* **1986**, *25*, 7725.
11. Bertho, G.; Ladam, P.; Gharbi-Benarous, J.; Delaforge, M.; Girault, J. P. *J. Chim. Phys.* **1998**, *95*, 423.
12. Bertho, G.; Gharbi-Benarous, J.; Ladam, P.; Delaforge, M.; Girault, J. P. *Bioorg. Med. Chem.* **1998**, *6*, 209.
13. Goldman, R. C.; Fesik, S. W.; Doran, C. C. *Antimicrob. Agents Chemother.* **1990**, *34*, 426.
14. Fernandez-Munoz, R.; Vazquez, D. *J. Antibiot.* **1973**, *26*, 107.
15. Pestka, S. *Antimicrob. Agents Chemother.* **1974**, *6*, 474.
16. Gharbi-Benarous, J.; Evrard-Todeschi, N.; Ladam, P.; Bertho, G.; Delaforge, M.; Girault, J. P. *J. Chem. Soc., Perkin Trans. 2* **1999**, 529.
17. Evrard-Todeschi, N.; Gharbi-Benarous, J.; Bertho, G.; Gaillet, C.; Lang, C.; Parent, A.; Girault, J. P. *Bioorg. Med. Chem.* **1999**, in press.
18. Bertho, G.; Gharbi-Benarous, J.; Delaforge, M.; Lang, C.; Parent, A.; Girault, J. P. *J. Med. Chem.* **1998**, *41*, 3373.
19. Barber, J.; Gyi, J. I.; Pye, D. A. *J. Chem. Soc., Chem. Commun.* **1991**, 1249.
20. Pye, D. A.; Gyi, J. I.; Barber, J. *J. Chem. Soc., Chem. Commun.* **1990**, 1143.
21. Gyi, J. I.; Brennan, R. J.; Pye, D. A.; Barber, J. *J. Chem. Soc., Chem. Commun.* **1991**, 1471.
22. Heman-Ackah, S. M.; Garrett, E. R. *J. Pharm. Sci.* **1972**, *61*, 545.
23. Chang, F. N. *Lincomycin*; Hahn, F. E., Ed.; New York, 1979; Vol. 5, pp 127.
24. Contreras, A.; Vazquez, D. *Eur. J. Biochem.* **1977**, *74*, 539.
25. Haasnoot, C. A. G.; De Leeuw, F.; Altona, C. *Tetrahedron* **1980**, *36*, 2783.
26. Tvaroska, I.; Hricovini, M.; Petrakova, E. *Carbohydrate Research* **1989**, *189*, 359.
27. Bendall, M. R.; Pegg, D. T. *J. Magn. Reson.* **1983**, *53*, 272.
28. Hurd, R. E.; John, B. K. *J. Magn. Reson* **1991**, *91*, 648.
29. Bax, A.; Summers, M. F. *J. Am. Chem. Soc.* **1986**, *108*, 2093.
30. Roberts, G. C. K.; Jardetzky, O. *Adv. Protein Chem.* **1970**, *24*, 447.
31. Jardetzky, O.; Roberts, G. C. K. *NMR in Molecular Biology*; Academic: New York, 1981.
32. Willker, W.; Leibfritz, D. *Magn. Reson. Chem.* **1995**, *33*, 632.
33. Allerhand, A.; Doddrell, D.; Komoroski, R. *J. Chem. Phys* **1971**, *55*, 189.
34. Leban, I.; Golic, L.; Resman, A.; Zmitek, J. *Acta Chim. Slov.* **1994**, *41*, 405.
35. Burt, S. K.; Mackay, D.; Nagler, A. T. *Computer-Aided Drug Design*, Perun, T. J., Propst, C. L. Eds., Marcel Dekker: Basel, New York, 1989.
36. Weiner, S. J.; Kollmann, P.; Case, D. A.; Singh, U. C.; Ghio, C.; Alagona, G.; Profeta, S.; Weiner, P. *J. Am. Chem. Soc.* **1984**, *106*, 765.
37. Hünenberger, P. H.; Mark, A. E.; van Gunsteren, W. F. *J. Mol. Biol.* **1995**, *252*, 492.
38. Alam, P.; Buxton, P. C.; Parkinson, J. A.; Barber, J. *J. Chem. Soc. Perkin Trans.* **1995**, *2*, 1163.
39. Bertho, G.; Ladam, P.; Gharbi-Benarous, J.; Delaforge, M.; Girault, J. P. *Int. J. Biol. Macromolecules* **1998**, *22*, 103.
40. Wuthrich, K.; Billeter, M.; Braun, W. *J. Mol. Biol.* **1983**, *169*, 949.
41. Shipman, L. L.; Christoffersen, R. E. *J. Med. Chem.* **1974**, *17*, 583.
42. Awan, A.; Brennan, R. J.; Regan, A. C.; Barber, J. *J. Chem. Soc., Chem. Commun.* **1995**, *16*, 1653.
43. Verdier, L.; Gharbi-Benarous, J.; Bertho, G.; Mauvais, P.; Girault, J.-P. *J. Chim. Phys.* **1999**, *96*, 1616.

44. Tritton, T. R. *Biochemistry* **1977**, *16*, 4133.
45. Garrett, R. A.; Rodriguez-Fonseca, C. *The Peptidyl Transferase Center*; CRC, 1996; pp 327.
46. Fournet, M. P.; Barre, J.; Zini, R.; Deforges, L.; Duval, J.; Tillement, J. P. *J. Pharm. Pharmacol.* **1987**, *39*, 319.
47. Dauber-Osguthorpe, P.; Roberts, V. A.; Osguthorpe, D. J.; Wolff, J.; Genest, M.; Hagler, A. T. *Proteins: Structure, Function and Genetics* **1988**, *4*, 31.
48. Dinur, U.; Hagler, A. T. *J. Chem. Phys.* **1989**, *91*, 2949.
49. Dinur, U.; Hagler, A. T. *J. Chem. Phys.* **1992**, *97*, 9161.